box, percent duration staying in the light box, numbers of the transition between light and dark box, and the first latency to enter the dark box were measured as indices.

2.4.5. Elevated plus maze test

The next day (day 14) after the L-D box test, an elevated plus maze test was conducted. The detailed protocol is shown in the supplementary information.

2.4.6. Auditory startle response

The next day after the L-D box test, an auditory startle response test was conducted for 2 days. The detailed protocol is shown in the supplementary information.

2.4.7. The Morris water maze test

Three days after the termination of the auditory startle response test (day 18), a series of the Morris water maze test began. The detailed protocol is shown in the supplementary information.

2.4.8. Classical fear conditioning

Three days after the termination of the Morris water maze test (day 25), a classical fear-conditioning test was conducted. This test consisted of three parts: a conditioning trial (day 25), a context test trial (day 26), and a cued test trial (day 27). Fear conditioning was carried out on a clear plastic chamber equipped with a stainless steel grid floor (34 cm × 26 cm × 30 cm [H]). A CCD camera was equipped on the ceiling of the chamber and was connected to a video monitor and computer. The grid floor was wired to a shock generator. White noise (65 dB) was supplied from a loudspeaker as an auditory cue (CS). The conditioning trial consisted of a 2-min exploration period followed by two CS-US pairings separated by 1 min each. A US (foot-shock: 0.5 mA, 2 s) was administered at the end of the 30-s CS period. A context test was performed in the same conditioning chamber for 3 min in the absence of the white noise at 24 h after the conditioning trial. Further, a cued test was performed in an alternative context with distinct cues; the test chamber was different from the conditioning chamber in brightness (almost 0–1 lx), color (white), floor structure (no grid), and shape (triangular). The cued test was conducted 24 h after the contextual test was finished and consisted of a 2-min exploration period (no CS) to evaluate the non-specific contextual fear followed by a 2-min CS period (no foot shock) to evaluate the acquired cued fear. Rate of freezing response of mice was measured as an index of fear memory.

2.5. Behavioral analysis: phase III

This analysis was performed at the Support Unit for Animal Experiment, RIKEN BSI. For this analysis, seven homozygous KO mice (*Wfs1*$^{-/-}$) and eight WT littermates (*Wfs1*$^{+/+}$) were analyzed. All were males aged 9 weeks at the initiation of the behavioral analysis. There was no significant difference of body weight at the initiation of the behavioral tests (WT, 25.2 ± 0.6 g; KO, 25.2 ± 0.5 g).

The analyses were performed in the order of social interaction, rotarod test, sucrose preference test, tail suspension test, forced swimming test, marble burying test, hot plate test, and tail flick test. Inter-test intervals were 1 day to a week. After each trial (except the auditory startle response and the water maze), apparatuses were wiped and cleaned by 80% alcohol and damp towel. For data acquisition, the Image J program was used after some modification.

2.5.1. Social interaction test (encounter method)

Subject mice were individually put into the center of a white-colored open field (40 cm × 40 cm × 30 cm [H]). Immediately after the introduction of the subject mouse, a target mouse was also introduced into the same open field. The duration of contact behavior was measured for 60 min to assess passive contact. Contact or separation of mice was expressed as "1" or "2" by computerized image analysis. If the two mice contacted, the software return value of "1," and if separated, return value "2." Thus, smaller number means higher contact. Data were collected and analyzed using a personal computer and commercially available software (Time HC; O'Hara, Tokyo, Japan).

2.5.2. Motor coordination and motor learning test (rotarod)

Mice were individually placed on a rotating rod (O'Hara, Tokyo, Japan) and the time each animal was able to maintain its balance walking on top of the rod was measured. The speed of the rotarod was 4 rpm (on the first day) or accelerated from 4 to 40 rpm over a 4-min period and 40 rpm another 1 min (day 2 to day 5). Mice were given a trial for 2 min (day 1) or four trials with a maximum time of 300 s (inter-trial intervals were 20–30 s). Time between placement and falling or revolving around the rod was recorded manually.

2.5.3. Sucrose preference test

Mice were tested for a 3-days 24-h test and 1-day 1-h test with water deprivation. The 24-h tests were free choice between two bottles, one with sucrose (3% in filtered water) and another with filtered water. To eliminate the side preference, the position of bottles was switched every 24 h. The consumption of water and sucrose solution was assessed daily. After the choice test, mice were deprived water for 24 h and then a 1-h choice test between water and sucrose was conducted.

2.5.4. Tail suspension test

Mice were individually hung by the tail using an adhesive tape placed approximately 1.5 cm from the tip of the tail attached to a wire and 30 cm above the floor. The duration of immobility was scored and analyzed using Image J TS (O'Hara, Tokyo, Japan) for 5 min.

2.5.5. Forced swimming test

Mice were individually placed for 15 min (day 1) or 5 min (day 2) in glass cylinders (30 cm high, 10 cm in diameter) containing 10 cm of water maintained at 23–25 °C. The duration of immobility was scored and analyzed using Image J software. The immobility time during the first 5 min was assessed.

2.5.6. Marble burying test

The test was performed in the test cage identical to their home cage with a 5-cm thick layer of bedding material (TEK-FRESH, Edstrom Industries, Waterford, WI, USA). Mice were habituated to fresh bedding for 30 min and then briefly returned to their home cage; 20 glass marbles (1.5 cm in diameter) were placed evenly on the bedding. Mice were then reintroduced into the test cage and the number of buried marbles (buried into the bedding over 2/3) was analyzed 30 min later.

2.5.7. Hot plate and tail flick test

In the hot plate test (Model MK-350C, Muromachi-kikai, Tokyo, Japan), mice were individually placed on the plate (52 ± 0.5 °C) enclosed in a translucent plastic wall, and the time between placement and licking of the paws and jumping was recorded manually as the response latency. A cut-off time was 90 s. Because most of the mice did not jump, latency to licking was used for statistical analysis.

In the tail flick test (Model MK-330B, Muromachi-kikai, Tokyo, Japan), mice were individually restricted on the radiant heat meter and focused heat was applied to the surface of the tail at 2–3 cm from its tip; the latency to reflexive removal of the tail from the heat was recorded manually as the tail flick latency. A cut-off time was 10 s.

In these tests, data were obtained by two observers, and the shorter scores were adopted as the response time.

2.5.8. Statistical analysis

For statistical analysis of behavioral analyses phases I–III, the Student's *t*-test, one-way ANOVA, and repeated measures ANOVA (RMANOVA) were used. When a significant effect was found by one-way ANOVA, Tukey post hoc comparisons were applied. When sphericity was rejected by the Mauchly test before the application of RMANOVA, the Greenhouse-Geisser estimate was used. Paired *t*-test and two-sample *t*-test were also used for post hoc analysis when necessary. These statistical analyses were performed using SPSS 11.0 for Windows (SPSS Japan, Tokyo, Japan). Significance levels were set at 0.05 (two-tailed); d.f., degree of freedom. Average and standard error of mean (S.E.M.) were presented for each experimental parameter in one group.

2.6. Immunohistochemistry

Because several computer programs predicted that mouse *Wfs1* protein would be cleaved around position 36, we used the following amino acid sequence, Glu^{39}–Gly^{53} as an antigen. A hexadecapeptide (CEPPRAPRPQADPSAG) was synthesized, purified using high-performance liquid chromatography, and conjugated to keyhole limpet hemocyanin (KLH). Five Balb/c mice were injected intraperitoneally with the KLH-conjugated peptide emulsified in complete Freund's adjuvant. Antiserum was obtained 1 week after boosting with the same antigen. We performed Western blot analysis to selected sensitive antiserum specific to *Wfs1* protein.

For immunohistochemical analysis using *WfS1* antibody, wild-type B6 mice aged 20–22 weeks were used. The mouse brain was fixed by perfusion of paraformaldehyde and embedded with paraffin. Coronal or sagittal sections with the thickness of 8 μm were sliced from paraffin-embedded mouse brain.

After deparaffinization and hydration, the slices were incubated for 10 min at 95 °C in sodium citrate buffer. Endogenous peroxidase activity was quenched by H_2O_2/methanol treatment. For blocking, 0.8% Block Ace (Dainippon Sumitomo Pharma, Osaka, Japan) in phosphate-buffered saline (PBS) was used. Anti-*WfS1* antiserum was used by 2500× dilution. For second antibody, biotinylated anti-mouse IgG (Vector Laboratories, Burlingame, CA, USA) was used. Peroxidase/DAB staining was performed by Vectastain Elite ABC kit (Vector Laboratories).

2.7. DNA microarray analysis

DNA microarray analysis was performed in two developmental stages, 12 and 30 weeks old. Eight homozygous *Wfs1* KO mice and 8 WT littermates were sacrificed at the age of 12 weeks. Seven homozygous *Wfs1* KO mice and five WT littermates were also analyzed at the age of 30 weeks.

The hippocampus was rapidly dissected, and total RNA samples were extracted from the hippocampi using TRIzol reagent (Invitrogen, Carlsbad, CA, USA). Microarray analysis was performed according to the manufacturer's protocol (Affymetrix, Santa Clara, CA, USA). Briefly, 5 μg total RNA of each sample was reverse-transcribed into cDNA, and biotinylated cRNA was synthesized from the cDNA by in vitro transcription. DNA microarray experiments were performed using Mouse Genome 430 2.0 GeneChips (Affymetrix). The hybridization signal on the chip was scanned by a GeneArray scanner and processed by GeneSuite software (Affymetrix). The probe sets labeled as "present" in 8 of 16 samples at 12 weeks old (24703/45101 probe sets) or in 5 of 12 samples at 30 weeks old (24455/45101 probe sets) were selected. The raw data were analyzed using MAS5 (Affymetrix) and then imported into GeneSpring 7.3 software (Silicon Genetics, Redwood, CA). The signal intensity of each probe set on the microarray was divided by its median value using GeneSpring 7.3 software.

For statistical analysis, the Mann–Whitney *U*-test was performed between the KO mice and their WT littermates, and $P < 0.05$ was considered statistically significant.

The probe sets were classified based on the information from GeneOntology (http://www.geneontology.org/) using GeneSpring software. For the GeneOntology analysis, the differentially expressed probes were selected. The categories showing overrepresentation at the level of $P < 0.05$ and containing 10 or more probe sets were selected.

2.8. Real-time quantitative polymerase chain reaction (RT-PCR) analysis

The representative probe sets that showed altered expression in the DNA microarray analysis of mouse brains were verified by RT-PCR. The cDNA used for the DNA microarray analysis was used. Primers and probes for Gapdh, cdc42ep5, Rnd1, Wnt2, and Garnl1 were commercially available by the Assay-on-Demand service (Applied Biosystems, Foster City, CA). The assays were carried out according to the protocols supplied by the manufacturer using 7900HT real-time PCR systems (Applied Biosystems). The relative values were calculated by measuring $\Delta C_t = C_t$ (each gene) $- C_t$ (Gapdh) for each sample in quadruplicate. For statistical analysis, one-tailed Mann–Whitney *U*-test was applied, and $P < 0.05$ was considered statistically significant.

3. Results

3.1. Wheel-running activity

To assess whether or not the *Wfs1* KO mice show bipolar disorder-like behavioral phenotypes, wheel-running activity of the *Wfs1* KO mice and WT littermates was recorded for a period up to 2 months. The levels of wheel-running activity and the circadian rhythm were assessed using male mice that were 34 weeks old at the initiation of this analysis (KO, $n = 11$; WT, $n = 9$). Average wheel-running activity per day of *Wfs1* KO mice during 28 days under the L-D condition did not differ from that of WT littermates (Fig. 1a; WT, 221.3 ± 64.7 [mean ± S.E.M.] counts; KO, 142.2 ± 57.6 counts, d.f. = 18, $U = 29$, $P = 0.21$ by Mann-Whitney *U*-test). Delayed activity

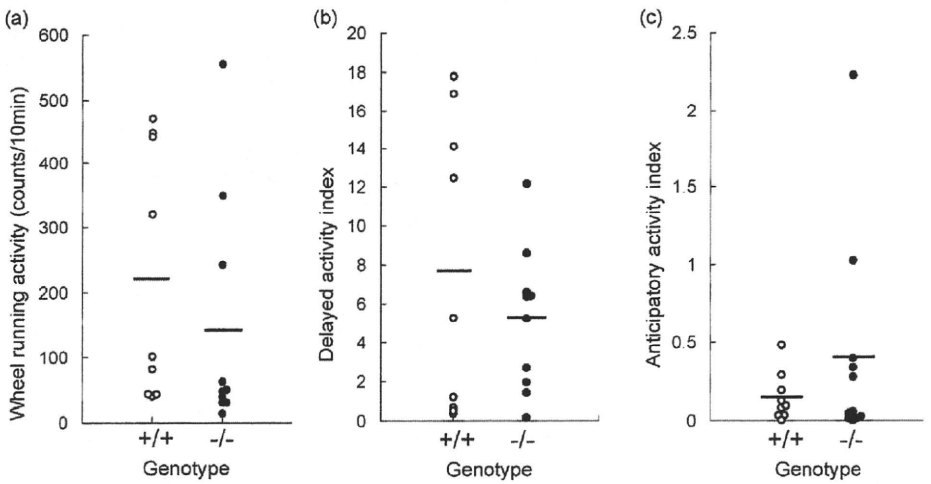

Fig. 1. Long-term wheel-running activity analysis. (a) Wheel-running activity. (b) Delayed activity index. Delayed activity index is defined as a percent of the wheel-running activity during the first 3 h of the light period with the total activity during the previous dark period (12 h). (c) Anticipatory activity index, the wheel-running activity in the last 3 h of light phase in comparison with the activity during dark phase. +/+, WT mice; −/−, *Wfs1* homozygous KO mice. Bars indicate averages. Each circle represents the datum of a mouse.

index (WT, 7.70 ± 2.50; KO, 5.29 ± 1.16, d.f. = 18, $U = 42$, $P = 0.84$) and anticipatory activity index (WT, 0.14 ± 0.05; KO, 0.34 ± 0.21, d.f. = 18, $U = 41$, $P = 0.78$) did not differ between the KO mice and WT littermates (Fig. 1a–c).

There was no abnormality of free running period measured at the constant dark condition in *Wfs1* KO mice (average 23.7 h, $n = 6$). None of female KO mice showed significant periodicity in wheel-running activity with the duration of 4–5 days (data not shown). These results show that the behavioral phenotypes of *Wfs1* KO mice are different from the mPolg Tg mice that exhibit altered circadian rhythm of wheel-running activity (Kasahara et al., 2006).

3.2. Behavioral analysis: phase I. Screening by a test battery

To screen the behavioral abnormality of *Wfs1* KO mice, we performed a conventional behavioral test battery using 14 homozygous KO mice, 14 heterozygous KO mice, and 13 WT littermates. The results of behavioral tests are summarized in Table 1.

3.2.1. Open-field test

Although a significant effect of time was found for both locomotor activity (d.f. = 8.6, $F = 3.0$, $P = 0.002$) and rearing (d.f. = 11.0, $F = 9.7$, $P = 0.000$), no significant effect of genotype was found for locomotor activity (d.f. = 2, $F = 0.70$, $P = 0.49$) and rearing (d.f. = 2, $F = 0.57$, $P = 0.56$). There was no significant interaction between time and genotype (locomotor, d.f. = 17.3, $F = 21.1$, $P = 0.57$; rearing, d.f. = 22.0, $F = 0.80$, $P = 0.71$) (Fig. 2a and b).

3.2.2. Startle response and prepulse inhibition

When RMANOVA was applied for the data of startle response, significant effect of blocks was found (d.f. = 5.12, $F = 7.80$, $P < 0.001$). However, no significant effect of genotype (d.f. = 2, $F = 0.664$, $P = 0.52$) or genotype × block block interaction (d.f. = 10.2, $F = 1.30$, $P = 0.22$) was found (Fig. 2c). No significant effect of genotype was found for the PPI ratio regardless of the interval of prepulse (50 ms, d.f. = 2, $F = 0.38$, $P = 0.68$; 100 ms, d.f. = 2, $F = 0.65$, $P = 0.52$; 200 ms, d.f. = 2, $F = 0.41$, $P = 0.66$, one-way ANOVA) (Fig. 2d).

3.2.3. Elevated plus maze

The number of entry into the open arms ($F = 0.31$, d.f. = 2, $P = 0.72$, one-way ANOVA) (Fig. 2e) and the time spent in the open arms ($F = 2.05$, d.f. = 2, $P = 0.14$) (Fig. 2f) were not significantly different among the genotypes. A significant effect of genotype was found for the total number of boluses ($F = 7.16$, d.f. = 2, $P = 0.002$) (Fig. 2g). The Tukey honest significant difference (HSD) test showed that homozygous KO mice had a significantly lower number of fecal boluses (2.7 ± 0.3 [mean ± S.E.M.]) compared with heterozygous KO mice (4.8 ± 0.5, $P = 0.01$) and WT mice (5.2 ± 0.5, $P = 0.004$).

Table 1
Summary of findings in behavioral tests

Test battery	Findings
Wheel-running activity (34 weeks, 11 KO, 9 WT)	
Periodicity	NS
Diurnal activity rhythm	NS
Phase I (12 weeks, 13 KO, 14 Hetero, 13 WT)	
Open field	NS
Startle/PPI	NS
Elevated plus maze	NS
Morris water maze	NS
Passive avoidance test	Longer latency to move
Active avoidance test	Reduced number of escape at day 3
Forced swimming test	Reduced immobility on the second day
Phase II (31 weeks, 9 KO, 11 WT)	
Home cage activity	NS
Open field	NS
Light-dark box	NS
Elevated plus maze	NS
Startle/PPI	NS
Morris water maze	Increased escape latency without the change of distance traveled
Fear conditioning	Enhanced freezing during conditioning and before the cue at the cue test
Phase III (9 weeks, 7 KO, 8 WT)	
Social interaction	Decreased interaction
Rota-rod	NS
Sucrose preference	NS
Tail suspension test	NS
Forced swimming test	Reduced immobility on the second day
Marble burying test	NS
Hot plate test	NS
Tail flick test	NS

KO, *Wfs1* (−/−); Hetero, *Wfs1* (−/+); WT, *Wfs1* (+/+). PPI: prepulse inhibition test, NS, non-significant.

3.2.4. Morris water maze

The time to reach the platform during the 5-day learning phase became shorter than the first day, shown by a significant effect of day by RMANOVA (d.f. = 4, $F = 19.1$, $P < 0.001$) (Fig. 2h). However, there was neither significant effect of genotype (d.f. = 2, $F = 0.56$, $P = 0.57$) nor significant interaction of day and genotype (d.f. = 2, $F = 0.53$, $P = 0.94$). The time spent in the target quadrant (d.f. = 2, $F = 0.10$, $P = 0.90$, one-way ANOVA) and immobility time (d.f. = 2, $F = 0.58$, $P = 0.56$) at the probe test performed on day 6 did not show a significant difference among the genotypes (Fig. 2i).

3.2.5. Passive avoidance test

The latency to escape at the conditioning phase was significantly different among the genotypes (d.f. = 2, $F = 4.70$, $P = 0.015$, one-way ANOVA). Multiple comparison showed that the latency in homozygous KO mice was significantly longer than that in WT mice ($P = 0.02$) (Fig. 3a). There was no significant difference in escape latency at the test session (d.f. = 2, $F = 0.81$, $P = 0.92$, one-way ANOVA).

3.2.6. Active avoidance test

The time course of mean escape latency was examined during 3-days' training, consisting of 5 blocks in each day

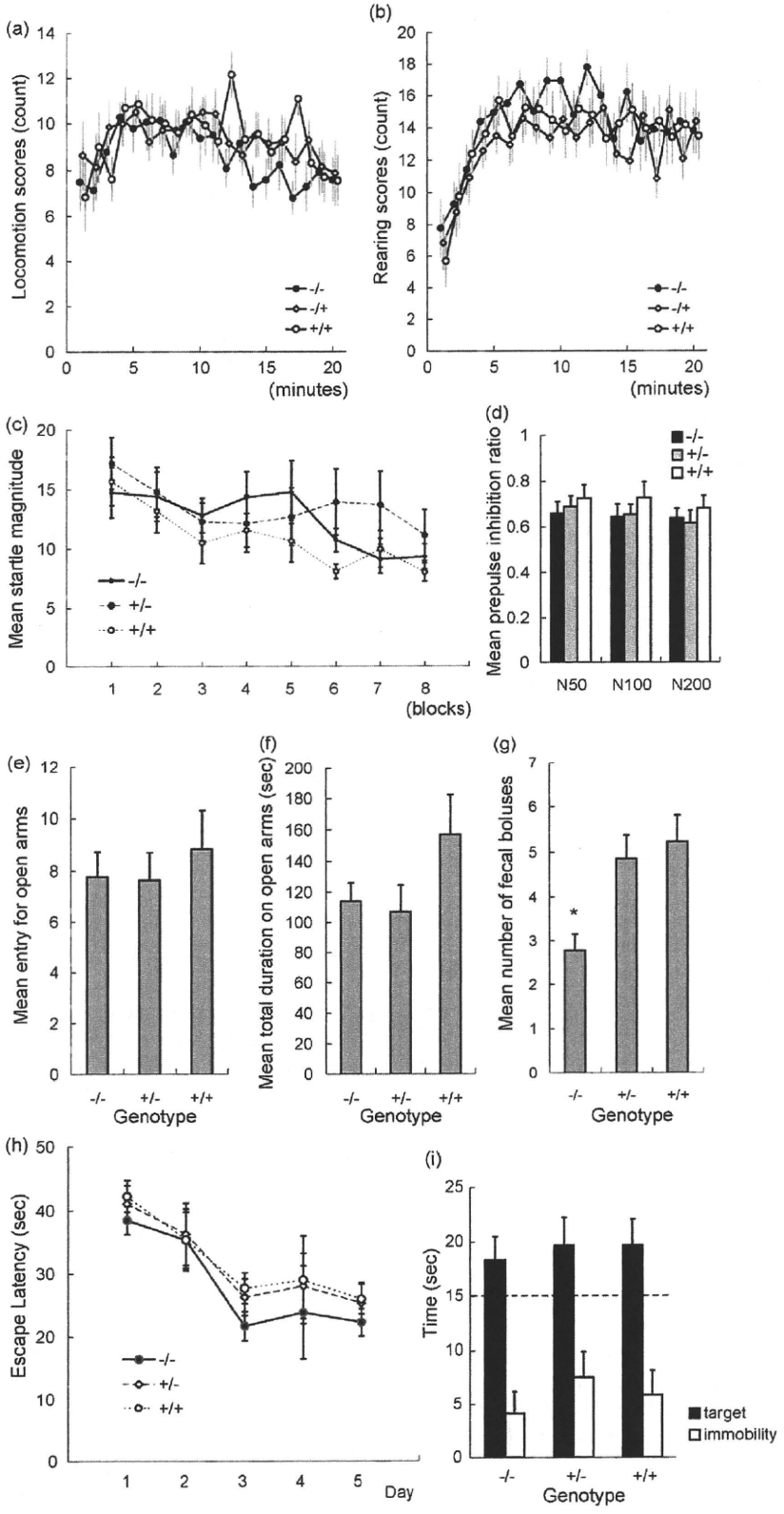

Fig. 2. Behavioral screening (1). (a–b) Open-field test. Locomotion scores (a) and rearing scores (b). Bars indicate the standard errors. (c) Startle response. (d) Prepulse inhibition test. N50 means the prepulse 50 ms before the startle pulse. (e–g) Elevated plus maze test. (h–i) Morris water maze test. Time course of escape latency during 5-days training (h), and time spent in the target quadrant during the 60-s session. Error bars represent standard error of mean. The dotted line represents the chance level. +/+, WT mice; +/−, *Wfs1* heterozygous KO mice; −/−, *Wfs1* homozygous KO mice. $^{*}P < 0.05$.

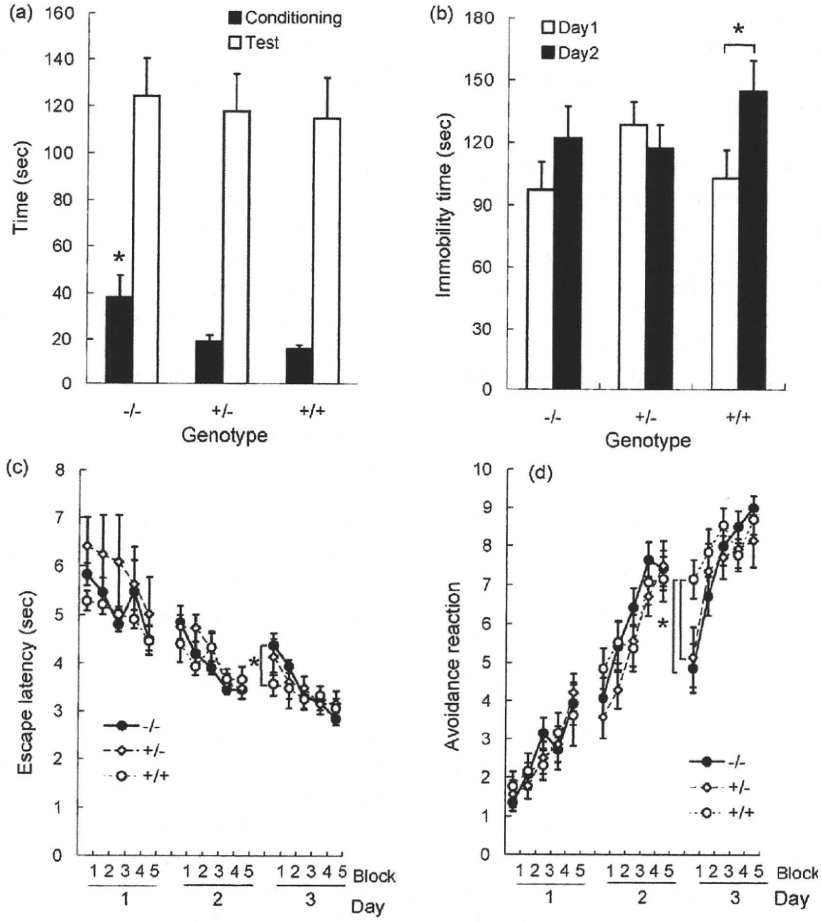

Fig. 3. Behavioral screening (2). (a) Passive avoidance test. (b) Forced swimming test performed on two sequential days. (c–d) Active avoidance test. +/+, WT mice; +/−, *Wfs1* heterozygous KO mice; −/−, *Wfs1* homozygous KO mice. Error bars represent standard error of mean. $^{*}P < 0.05$.

(Fig. 3c). In the three-way RMANOVA with the within-group factors of day and block and the between-group factor of genotype, although no significant effect of genotype was found (d.f. = 2, $F = 0.75$, $P = 0.47$), there was a significant interaction between genotype and block (d.f. = 1.75, $F = 2.94$, $P = 0.007$). No other two-way or three-way interactions were statistically significant. This significant interaction may be caused by longer escape latency of KO mice only at the first block. A post hoc analysis showed that the escape latency of the homozygous KO mice at the first block on day 3 was significantly longer than that in WT mice (d.f. = 25, $t = 2.34$, $P = 0.027$, with no correction for multiple comparison).

Similar interaction between genotype and block was also seen for the numbers of avoidance (d.f. = 6.3, $F = 3.25$, $P = 0.004$) (Fig. 3d). Both homozygous and heterozygous KO mice showed significantly lower numbers of avoidance at the first block on day 3 (homozygotes, d.f. = 25, $t = -2.82$, $P = 0.009$; heterozygotes, d.f. = 25, $t = -2.15$, $P = 0.04$).

3.2.7. *Forced swimming test*

When the immobility time was analyzed by RMANOVA, a significant effect of day (d.f. = 1, $F = 5.5$, $P = 0.024$) and a significant interaction of day and genotype (d.f. = 2, $F = 3.8$, $P = 0.031$) were found, whereas no significant effect of genotype was found (d.f. = 2, $F = 0.48$, $P = 0.61$) (Fig. 3b).

In the WT mice, immobility time was significantly longer on the second day (144.6 ± 53.0 s) compared with the first day (103.0 ± 48.3 s, d.f. = 12, $t = -3.45$, $P = 0.005$, paired t-test), possibly reflecting the learned despair (Parra et al., 1999). On the other hand, such a significant increase of immobility time on the second day was not observed for heterozygous (day 1, 128.5 ± 39.4 s; day 2, 117.5 ± 39.4 s; d.f. = 12, $t = 1.11$, $P = 0.28$) and homozygous (day 1, 97.4 ± 50.6 s; day 2, 122.0 ± 57.0 s; d.f. = 13, $t = -1.44$, $P = 0.17$) KO mice (Fig. 3b).

3.2.8. *Summary of the phase I behavioral analysis*

The results of the phase I behavioral analysis are summarized as follows.

(1) There was no abnormality in open field, elevated plus maze, PPI, and Morris water maze. However, it cannot be ruled out that the mice develop behavioral phenotypes at later age because depression is an adult-onset disease.
(2) The passive avoidance test showed the longer latency to enter the other chamber in *Wfs1* KO mice. This could be

explained either by low anxiety or retardation, that is slow movement or delayed onset of motion. However, it is also possible that mice could have been just busy exploring the first box, or they had some kind of place neophobia.

(3) The active avoidance test showed longer escape latency and lower numbers of avoidance at the first block on day 3 in *Wfs1* KO mice. This might suggest that the emotional memory is impaired in the *Wfs1* KO mice. It cannot be excluded, however, that *Wfs1* KO mice have impairment of pain sensitivity.

(4) Altered response to serial forced swimming test. This may suggest that the *Wfs1* KO mice tend to be resistant to behavioral despair.

3.3. Behavioral analysis: phase II

To further characterize the behavioral phenotypes of *Wfs1* KO mice, additional behavioral analysis was performed.

3.3.1. Open-field, elevated plus maze, PPI tests, and Morris Water Maze at 31 weeks

At first, four of behavioral tests were repeated in the mice aged 31 weeks to assess the effect of age. There were no significant difference between WT mice and *Wfs1* KO mice for three of these behavioral tests: open-field, elevated plus maze, and PPI tests (data not shown).

On the other hand, the Morris water maze test showed longer escape latency. Two-way RMANOVA showed significant effects of genotype (d.f. = 1, $F = 9.04$, $P = 0.008$) and day (d.f. = 3, $F = 8.45$, $P < 0.001$) (Fig. 4a). The *Wfs1* KO mice showed longer escape latency than controls. There was no significant interaction between genotype and day (d.f. = 3, $F = 0.60$, $P = 0.61$). On the other hand, there was no significant effect of genotype on the distance (d.f. = 1, $F = 0.38$, $P = 0.54$) (Supplementary Fig. 1a). Effect of day was significant (d.f. = 3, $F = 25.2$, $P < 0.001$), but the interaction between genotype and day was not significant (d.f. = 3, $F = 0.71$, $P = 0.54$). To assess the speed of swimming, a new index, swimming speed index = (total distance)/(latency to reach platform) was calculated. Two-way RMANOVA showed no significant effects of day (d.f. = 1.77, $F = 2.57$, $P = 0.09$) and genotype (d.f. = 1, $F = 0.04$, $P = 0.83$). There was no significant day × genotype interaction (d.f. = 1.77, $F = 0.33$, $P = 0.69$) (Supplementary Fig. 1b). Spatial memory cannot be assessed because no significant difference was found between the time spent in the target quadrant and that in the other three quadrants, suggesting that the probe test did not work properly even for wild-type mice (data not shown).

3.3.2. Home cage activity

To assess the general activity level, home cage activity was recorded for 8 days. When RMANOVA was applied, a significant effect of day (d.f. = 5, $F = 5.95$, $P < 0.001$) was found. There was no significant effect of genotype (d.f. = 1, $F = 0.61$, $P = 0.44$) and genotype × day interaction (d.f. = 5, $F = 0.53$, $P = 0.75$) (Fig. 4b).

3.3.3. Anxiety-like behavior

Next, the level of anxiety-like behavior was further assessed by the L-D box. The marble burying test was also performed in the 9-week-old mice in the phase III behavioral analysis.

In the L-D box test, no significant difference was found in the time spent in the light box (WT, 39.2 ± 9.0%, KO, 37.1 ± 9.8%, d.f. = 18, $t = 0.50$, $P = 0.61$). There was no significant difference in the number of marbles buried (WT 16.0 ± 0.8, KO 17.1 ± 0.7, $t = 1.0$, $P = 0.33$). These findings suggest that longer latency to escape at the passive avoidance test was not due to lower anxiety-like behavior.

3.3.4. Emotional memory

To test the hypothesis that emotional memory is impaired in the *Wfs1* KO mice, the fear conditioning test was performed.

During the conditioning phase, two-way RMANOVA revealed significant effect of genotype (d.f. = 1, $F = 4.47$, $P = 0.049$) and time (d.f. = 3.54, $F = 22.1$, $P < 0.001$). No significant period × genotype interaction was found (d.f. = 3.54, $F = 1.73$, $P = 0.16$). The *Wfs1* KO mice showed significantly longer time of freezing during the conditional stimuli (periods 5 and 7) and at the final period (Student's *t*-test, $P < 0.05$) (Fig. 4c).

For the cue test, two-way RMANOVA was applied to the data set before and after the cue, separately. For the data of freezing before the cue, a slight tendency of the effect of genotype (d.f. = 1, $F = 2.9$, $P = 0.10$) was seen, whereas there was significant effect of time (d.f. = 3, $F = 5.93$, $P = 0.001$) and no interaction between genotype and time (d.f. = 3, $F = 0.30$, $P = 0.82$). The *Wfs1* KO mice spent a significantly longer time for freezing ($t = 2.48$, $P < 0.01$) (Fig. 4d). However, no significant effect of genotype was found after the cue (effect of genotype, d.f. = 1, $F = 1.48$, $P = 0.23$; effect of time, d.f. = 3, $F = 1.60$, $P = 0.19$; genotype × time interaction, d.f. = 3, $F = 0.40$, $P = 0.75$). There was no significant effect of genotype at the context test (Fig. 4e).

These findings suggested that memory of emotion is not impaired in the *Wfs1* KO mice.

3.4. Behavioral analysis: phase III

3.4.1. Pain sensation

As noted above, it cannot be excluded that *Wfs1* KO mice have impairment of pain sensitivity. To rule out such possibility, the hot plate test and tail flick test were performed. No difference in the latency to licking (WT, 10.3 ± 1.2 s; KO, 9.9 ± 0.9 s, $t = 0.219$, d.f. = 12, $P = 0.83$, by Student's *t*-test) was found between the *Wfs1* KO mice and WT mice by the hot plate test. There was no significant difference in the latency to flick the tail (WT, 3.5 ± 0.2 s; KO, 3.4 ± 0.2 s, d.f. = 12, $t = 0.29$, $P = 0.77$).

3.4.2. Motor function

As noted above, many of the positive findings in behavioral tests can be interpreted as reflecting retardation. Such findings can be explained by altered motor functions, such as impairment in muscle contraction, voluntary movement, or

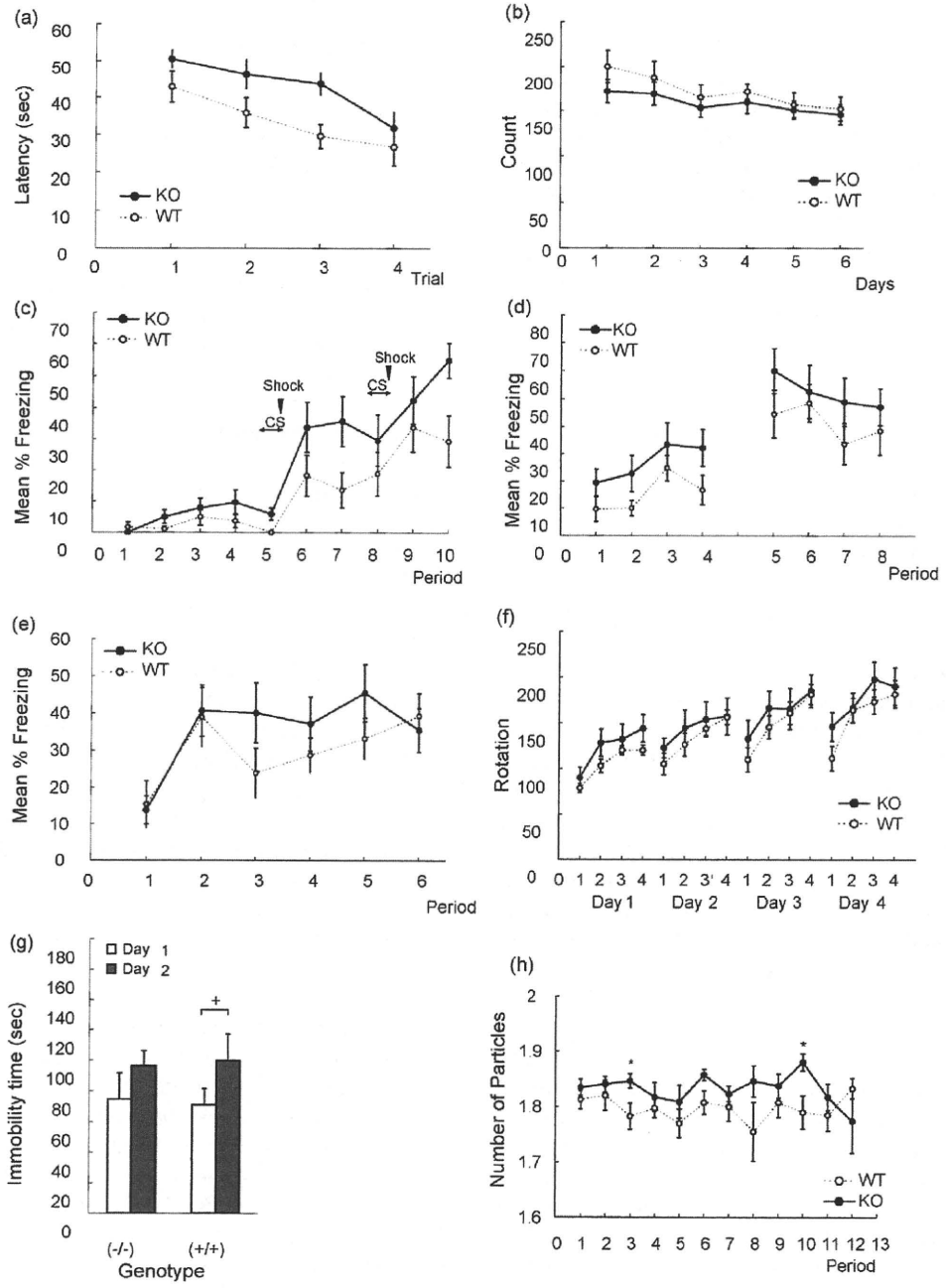

Fig. 4. Further characterization of behavioral phenotypes of *Wfs1* KO mice. (a) Morris water maze test. (b) Home cage activity. (c and d) Fear conditioning test. One time period is 30 s. (c) Conditioning phase. Conditional stimuli (tone) and unconditional stimuli (foot shock) were applied during periods 5 and 8. (d) Cue test. Cue was applied between the time periods 4 and 5. (e) Context test. (f) Rotarod test. (g) Forced swimming test. (h) Social interaction test. Note that high number of particles indicates lower levels of social interaction.

motor coordination. To test this possibility, the rotarod test was performed. Three-way RMANOVA with the intra-individual factors of day and trial and inter-individual factor of genotype showed no significant effect of genotype (d.f. = 1, $F = 1.02$, $P = 0.33$). Whereas significant effects of day (d.f. = 3, $F = 15.6$, $P < 0.001$) and trial (d.f. = 3, $F = 51.0$, $P < 0.001$) were found, no significant two-way or three-way interactions were detected except for a trend of interaction between day and trial (d.f. = 3, $F = 2.54$, $P = 0.07$) (Fig. 4f).

3.4.3. Behavioral despair

As noted above, *Wfs1* KO mice showed altered response to the serial forced swimming test. To further confirm this finding, the forced swimming test was performed again.

RMANOVA revealed a tendency of effect of day (d.f. = 1.0, $F = 3.83$, $P = 0.07$). There was no significant effect of genotype (d.f. = 1, $F = 0.18$, $P = 0.67$) and day × genotype interaction (d.f. = 1.0, $F = 0.17$, $P = 0.68$).

Although no day × genotype interaction was found in this analysis, the paired *t*-test was applied similarly to the first experiment (Fig. 4g). Immobility time tended to be longer on the second day (99.7 ± 17.4 s) compared with the first day (71.0 ± 10.55 s, $r = 0.68$, $P = 0.064$, paired *t*-test) in WT mice, whereas no significant difference was found in *Wfs1* KO mice (day 1, 74.5 ± 17.1 s; day 2, 96.2 ± 10.0 s, $r = 0.50$, $P = 0.24$). This analysis showed a similar tendency to the first experiment.

The other test of behavioral despair, the tail suspension test, was also performed. There was no significant difference in the immobile time between the *Wfs1* KO mice and WT mice (WT, 9.0 ± 2.8%; KO, 9.4 ± 3.0%, $t = 0.09$, $P = 0.92$).

3.4.4. Other aspects of depression

Some of these noted findings in the *Wfs1* KO mice can be explained by the retardation in emotionally triggered motion. This could not be explained by abnormalities in instrumental motor functions. Such findings seem to be similar to "psychomotor retardation" seen in human depressive patients. Though the findings in the forced swimming test and tail suspension test are equivocal, behavioral despair is not always a valid depression model. Thus, we further examined the other aspects of depression.

The sucrose preference test is an established test for anhedonia, one of the core symptoms of depression. In the choice test for 3 days, there was no significant effect of genotype (d.f. = 1, $F = 0.95$, $P = 0.34$) by two-way RMANOVA (WT, day 1, 44.2 ± 16.7%, day 2, 94.1 ± 5.2%, day 3, 84.5 ± 9.7%; KO, day 1, 37.3 ± 12.9%, day 2, 97.3 ± 1.7%, day 3, 60.2 ± 16.0%). A significant effect of trial (d.f. = 2, $F = 10.7$, $P = 0.001$) and no significant interaction of genotype × trial was found (d.f. = 2, $F = 0.68$, $P = 0.51$). The 1-h choice test after 24-h water deprivation did not show a significant difference between genotypes (WT 90.2 ± 1.7%, KO 86.3 ± 5.3%, $U = 28$, NS).

The social interaction test is an established test for anxiety-like behavior (File and Seth, 2003). However, its response to drugs is different from elevated plus maze, and it is more sensitive to serotonergic drugs. Recently, this test is also applied to animal models of schizophrenia (Miyakawa et al., 2003) and autism, and to genetic models of anxiety and depression (Overstreet et al., 2003). Thus, social behavior of the *Wfs1* KO mice was examined by this test. Two-way RMANOVA revealed no significant effect of genotype (d.f. = 1, $F = 2.0$, $P = 0.17$) and time (d.f. = 11, $F = 0.93$, $P = 0.51$). There was a trend of genotype × time interaction (d.f. = 11, $F = 1.67$, $P = 0.08$) (Fig. 4h). The *Wfs1* KO mice showed significant decrease of social interaction at the periods 3 and 10 (Student's *t*-test, $P < 0.05$) shown by the higher number of particles observed.

3.5. Wfs1 immunohistochemistry

To determine the molecular basis of behavioral abnormality in *Wfs1* KO mice, we verified whether the distribution of *Wfs1* protein in the brains of WT B6 mice is similar to that in rats (Fig. 5a–f) (Takeda et al., 2001). We verified that no staining was observed in *Wfs1* KO mice, suggesting the specificity of the anti-*Wfs1* antibody (Fig. 5g).

Wfs1-like immunoreactivity (*Wfs1*-IR) localized mostly to neurons and its regional distribution was mostly similar to that in rats (Fig. 5a). *Wfs1*-IR was most abundant in the hippocampal CA1 pyramidal neurons (Fig. 5b), and strong in the layer II pyramidal neurons of the cerebral cortex (Fig. 5c). Similar to rats, *Wsf1*-IR was also rich in the striatum, nucleus accumbens, thalamus, cerebellar Purkinje cells, amygdala, and bed nucleus of the stria terminalis (Fig. 5d). In addition, *Wfs1*-IR was observed in several hypothalamic nuclei, such as the paraventricular nucleus and suprachiasmatic nucleus (SCN) in mice (Fig. 5e). In the adjacent region of SCN, sub-paraventricular zone, some cell bodies showed *Wfs1*-IR. The ventromedial nucleus and arcuate nucleus also showed *Wfs1*-IR (Fig. 5f). *Wfs1*-IR was also found in the locus coeruleus and cochlea nucleus (data not shown).

3.6. DNA microarray analysis

To examine what sort of functional impairment occurs in the neurons of *Wfs1* KO mice, we performed gene expression analysis using DNA microarray. Because *Wfs1*-IR was most abundant in hippocampus, we performed DNA microarray analysis in the hippocampus of the *Wfs1* KO mice. A total of 1012 probe sets were changed at the age of 12 weeks. To narrow down the gene list, we repeated the experiment at the age of 30 weeks. We assumed that the true gene expression difference observed at age 12 weeks should be replicated at age 30 weeks. At the age of 30 weeks, 3508 probe sets showed significant differences. The genes altered in the same direction at both the ages of 12 and 30 weeks, and the fold change higher than 1.2 are shown in Table 2.

GeneOntology (GO) analysis showed that genes related to ribosome biogenesis (GO:3735: structural constituent of ribosome, GO:7046: ribosome biogenesis, GO:3723: RNA binding) or other basic cellular functions (GO:5622: intracellular, GO:44249: cellular biosynthesis, GO:15399: primary active transporter activity, GO:5623: cell, GO:7028: cytoplasm organization and biogenesis) were commonly up-regulated at the age of 12 and 30 weeks (Supplementary Tables 1 and 2). The major difference between the weeks 12 and 30 is the inclusion of neurodevelopment-related genes at the age of 30 weeks (GO:48666: neuron development, GO:30182: neuron differentiation, GO:7409: axonogenesis, GO:48667: neuron morphogenesis during differentiation, and GO:31175: neurite morphogenesis) (Supplementary Table 2).

3.7. RT-PCR analysis

To test whether the findings by DNA microarray analysis are chance findings, RT-PCR analysis was performed. For this purpose, two down-regulated genes, *cdc42ep5* and *Rnd1*, as well as two up-regulated genes, *Wnt2* and *Garnl1*, were examined using Gapdh as a reference.

The level of cdc42ep5 and Rnd1 tended to be lower at 12 weeks but not at 32 weeks. On the other hand, Wnt2 and Garnl1

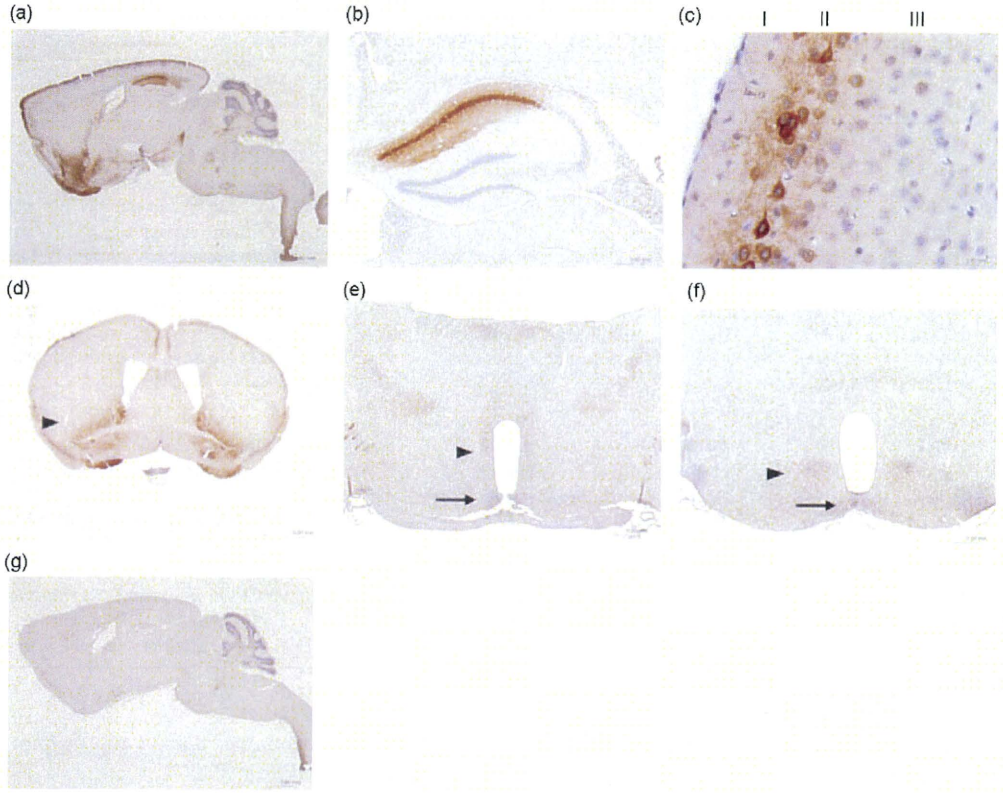

Fig. 5. Localization of *Wfs1*-like immunoreactivity in mouse brain. Immunohistochemistry analysis of mouse brain using anti-*Wfs1* antiserum. Coronal sections are shown except for panel a. (a) Sagittal section of the whole brain. (b) Hippocampus. CA1 (corpus ammon 1) region is selectively stained. (c) Cerebral cortex. Layer II pyramidal neurons are stained. (d) Coronal section at the level of bed nucleus of striata terminalis (BNST). At this level, the regions with intense *Wfs1*-IR looked as if they are surrounding the internal capsule (arrowhead). (e and f) Hypothalamus. Suprachiasmatic nucleus and sub-paraventricular zone are indicated by an arrow and an arrowhead, respectively (e). Arcuate nucleus and ventromedial nucleus are shown by an arrow and an arrowhead, respectively (f). (g) Immunohistochemistry analysis of the brain of a *Wfs1* KO mouse using anti-*Wfs1* antiserum. No staining is detected.

were significantly up-regulated at 32 weeks but not at 12 weeks (Table 3).

4. Discussion

4.1. Behavioral analyses

We recently reported that mPolg Tg mice show bipolar disorder-like behavioral phenotypes, such as altered circadian rhythm in both males and females and periodic fluctuation of wheel-running activity in females (Kasahara et al., 2006). Based on previous reports suggesting that patients with Wolfram disease are frequently affected with depression or bipolar disorder, we speculated that the *Wfs1* KO mice might also show these bipolar disorder-like phenotypes, which were seen in the mPolg Tg mice. However, *Wfs1* KO mice did not show similar phenotypes (Fig. 1).

Thus, we next examined the possibility that *Wfs1* KO mice show other types of behavioral phenotypes. At first, a battery of established behavioral tests was applied. There was no marked difference found in most of conventional behavioral tests, such as the open-field test, startle response, prepulse inhibition test, and elevated plus maze. The lack of marked difference in these tests was replicated in the mice aged 31 weeks. On the other hand, several tests in the initial test battery showed equivocal findings. In the passive avoidance test, the mice showed longer latency to move into the dark compartment at the training phase (Fig. 3a). The active avoidance test showed subtle differences between the KO and WT mice. On the third day of training, WT mice kept the same level of escape latency and number of avoidance reactions as the final block of the second day. Although, *Wfs1* KO mice seemed as if they forget the previous memory of escape training (Fig. 3c and d), it is unlikely considering the fact that there were no differences in the day 2 of the active avoidance test and in the contextual testing of the fear conditioning test. Otherwise, they may remember the events, but could not take the adequate action under the situation for some other reasons. For example, a possibility is that they showed retardation or increased behavioral despair without any problems in memory retention. In the forced swimming test performed for two sequential days, WT mice showed an increase of immobility time on the second day (Fig. 3d). This is in accordance with a previous study showing that mice became immobile on the second day of the sequential forced swimming test (Parra et al., 1999). This phenomenon was not observed in the homozygous and heterozygous KO mice (Fig. 3d). Although statistical analysis did not show the same difference, a similar tendency was observed in the second

Table 2
Probe sets commonly altered both at 12 and 30 weeks

Probe set ID	*P*-value		Fold change		Gene symbol	chromosome	Gene title
	12W	30W	12W	30W			
Down							
1433815 at	0.0008	0.0074	−2.24	−1.72	Jakmip1	5qB3[a]	Janus kinase and microtubule interacting protein 1
1448411 at	0.0008	0.0045	−2.10	−2.00	*Wfs1*	5qB3[a]	Wolfram syndrome 1
1419744 at	0.0357	0.0424	−1.45	−1.44	H2-DMb2	17qB1	Histocompatibility 2, class II, locus Mb2
1442241 at	0.0357	0.0424	−1.41	−1.49	Srpk2	5qA3[a]	Serine/arginine-rich protein specific kinase 2
1425620 at	0.0157	0.0284	−1.39	−1.22	Tgfbr3	5qE5[a]	Transforming growth factor, beta receptor III
1418712 at	0.0274	0.0284	−1.36	−1.47	Cdc42ep5	7qA1	CDC42 effector protein (Rho GTPase binding) 5
1441317 x at	0.0011	0.0045	−1.34	−1.71	Jakmip1	5qB3[a]	Janus kinase and microtubule interacting protein 1
1455197 at	0.0357	0.0424	−1.26	−1.29	Rnd1	15qF1	Rho family GTPase 1
Up							
1418148 at	0.0087	0.0074	2.03	1.68	Abhd1	5qB1[a]	Abhydrolase domain containing 1
1431328 at	0.0046	0.0424	1.50	1.21	Ppp1cb	5qB1[a]	Protein phosphatase 1, catalytic subunit, beta isoform
1459714 at	0.0157	0.0284	1.35	1.57	–	4qE1	–
1449425 at	0.0357	0.0074	1.28	1.28	Wnt2	6qA2	Wingless-related MMTV integration site 2
1457532 at	0.0357	0.0185	1.27	1.35	Garnli	12qC1	GTPase activating RANGAP domain-like 1
1416569 at	0.0274	0.0118	1.25	1.24	Actl6a	3qA3	Actin-like 6A
1446406 at	0.0460	0.0424	1.24	1.20	Paqr8	1qA4	Progestin and adipoQ receptor family member VIII
1446815 at	0.0357	0.0424	1.23	1.29	Dph4	2qE3	DPH4 homolog (JJJ3, S. cerevisiae)
1456328 at	0.0460	0.0284	1.22	1.33	Bank1	3qG3	B-cell scaffold protein with ankyrin repeats 1

[a]The probe sets on the chromosome 5.

forced swimming test. In addition, the other test for behavioral despair, the tail suspension test, did not show any significant difference. On the other hand, the longer escape latency of the KO mice without the difference of the distance traveled in the Morris water maze might reflect the longer time for immobility during the session. Thus, the *Wfs1* KO mice might show enhanced or attenuated behavioral despair depending on experimental conditions.

Table 3
Validation study of gene expression using RT-PCR

Gene	Genotype	N	Average	S.E.M.	*P*-value
12w					
cdc42ep5	WT	8	0.68	0.02	
	KO	8	0.63	0.02	0.088*
Rnd1	WT	8	0.42	0.01	
	KO	8	0.39	0.02	0.070*
Wnt2	WT	8	0.42	0.01	
	KO	8	0.44	0.02	0.227
Garnl1	WT	8	15.30	0.37	
	KO	8	14.62	0.61	0.180
32w					
cdc42ep5	WT	5	0.63	0.01	
	KO	7	0.66	0.03	0.225
Rnd1	WT	5	0.58	0.04	
	KO	7	0.54	0.04	0.235
Wnt2	WT	5	0.40	0.01	
	KO	7	0.44	0.02	0.041**
Garnl1	WT	5	12.95	0.16	
	KO	7	14.37	0.64	0.049**

The gene expression levels were normalized by Gapdh. Each value represents the gene/Gapdh ratio × 10^{-2}. *P*-values were calculated by Mann–Whitney *U*-test (one tailed).
* $P < 0.10$
** $P < 0.05$.

As described above, it was speculated that longer latency to move at the passive avoidance test can be explained either by low anxiety or retardation of *Wfs1* KO mice. The former possibility was not supported by two established tests for anxiety-like behavior, the L-D box test, and the marble burying test.

Wfs1 KO mice also showed longer escape latency and lower numbers of avoidance during the active avoidance test. This was not due to decreased pain sensitivity. This cannot be explained by the impairment of emotional memory, because there was no significant abnormality in fear conditioning test. This test instead showed increased freezing during conditioning phase. Freezing was also increased during the cue test, not after the cue but before the cue.

The *Wfs1* KO mice did not show impairment in fundamental motor functions that can explain these findings.

In summary, the following findings were obtained.

(1) Longer latency to move in passive avoidance test.
(2) Diminished avoidance reaction during active avoidance test.
(3) Longer escape latency in Morris water maze.
(4) Increased freezing during conditioning.
(5) Normal sensorimotor function and anxiety-like behavior.

These findings together suggest that the *Wfs1* KO mice might show retardation in the emotionally triggered motion. We could not discriminate whether this feature of the *Wfs1* KO mice reflects the slow movement, longer time to initiate movement, or mixture of both. Psychomotor retardation, that is, slow voluntary movement and thoughts and/or taking longer

time to initiate movement, is one of the characteristic symptoms of melancholic depression. The observed retardation of the *Wfs1* KO mice resembled such a characteristic symptom of depression. Thus, other aspects of depression were also examined. Although, the sucrose preference test did not show any difference, the social interaction test showed decreased social interaction in *Wfs1* KO mice.

Together these results suggest that *Wfs1* KO mice have some similarity to patients with depressive disorder. It should be noted, however, that the observed difference in the social interaction test might also reflect the retardation noted above. The *Wfs1* KO mice did not show marked abnormalities in the conventional behavioral despair paradigm, such as the forced swimming test and tail suspension test. These tests are established as screening tests for compounds having tricyclic antidepressant-like properties. However, its construct validity as a depression model is questioned (Crawley, 2007).

Taken together, the *Wfs1* KO mice show behavioral alterations at least partly mimicking the symptoms of depression. Further studies to examine the effects of antidepressive agents would be extremely interesting.

4.2. Morphologic analyses

Immunohistochemistry demonstrated that the distribution of *Wfs1*-IR was similar to that in rats (Fig. 5) (Takeda et al., 2001). In addition, we found that *Wfs1*-IR is also present in the hypothalamus. The presence of *Wfs1*-IR in the arcuate nucleus seems to be in accordance with diabetes insipidus, the major symptom of Wolfram disease. In a similar way, *Wfs1*-IR in the cochlea nucleus may be relevant to deafness in patients with Wolfram disease. It is also interesting that *Wfs1*-IR is found in the locus coeruleus and substantia nigra, from which noradrenergic and dopaminergic fibers originate. In *Wfs1* KO mice, however, we did not observe marked morphologic alterations in these regions using hematoxylin–eosin staining and Kluver-Barrera staining (data not shown).

4.3. Gene expression analysis

The fact that *Wfs1* itself is included in the list of altered genes (Table 2) supports the validity of our experiment and data analysis. Among the eight down-regulated and nine up-regulated genes, six other genes in addition to *Wfs1* itself were on the chromosome 5. This is possibly caused by residual genomic region derived from the 129Sv mice. Thus, only a part of these changes can be attributable to the absence of *Wfs1* itself. The present result is in accordance with a previous report that there were only small differences in expression profiles seen in fibroblasts obtained from patients with Wolfram disease (Philbrook et al., 2005).

Among the three down-regulated genes outside chromosome 5, two (*Cdc42ep5* and *Rnd1*) were related to Rho GTPase. Down-regulation of Rnd1 was validated at the age of 12 weeks but not at 32 weeks.

Cdc42ep5 encodes CDC42 effector protein. CDC42 plays a role in dendrite development (Threadgill et al., 1997). *Cdc42ep5* is one of the targets of CDC42 (Joberty et al., 1999), but its function in neurons is not known yet. *Rnd1* also plays a role in activity-dependent dendrite development (Ishikawa et al., 2006). A recent fine mapping analysis of 13q33 in bipolar disorder revealed the linkage with DOCK9, an activator of Cdc42 (Detera-Wadleigh et al., 2007). This finding also suggested the possible role of Rho GTPase in mood disorder. Together with the GO analysis showing altered neural development related genes at age 30 weeks, these findings may suggest that dendrite development may be impaired in *Wfs1* KO mice. Although, we did not observe morphologic difference between *Wfs1* KO mice and WT littermates using hematoxylin–eosin staining and Kluver-Barrera staining, dendrite morphology cannot be assessed using these methods. Further analysis by Golgi staining or other methods might be promising.

Up-regulation of two genes were validated at 32 weeks but not at 12 weeks. Up-regulation of Wnt2 is potentially interesting because Wnt signaling plays a role in neural plasticity and is implicated in the molecular pathology of bipolar disorder (Gould and Manji, 2002; Matigian et al., 2007).

Up-regulation of ribosome-related genes at both 12 and 30 weeks revealed by gene ontology analysis might be in accordance with the putative role of *WfS1* in ER stress response (Fonseca et al., 2005; Yamada et al., 2006).

4.4. Phenotypic discordance between Wfs1 KO mice and patients with Wolfram disease

In this study, *Wfs1* KO mice did not show marked sensorimotor and general health problems that are seen in patients with Wolfram disease. This is in accordance with the lack of spontaneous diabetes mellitus in *Wfs1* KO mice on the B6 background (Ishihara et al., 2004). Although, we detected some behavioral phenotypes in KO mice, it cannot be ruled out that some of detected behavioral alterations in *Wfs1* KO mice could be explained by the residual genomic region derived from 129Sv mice (Mouse Phenome Database, http://phenome.jax.org/pub-cgi/phenome/mpdcgi?rtn=docs/home).

It is possible that the symptoms in patients with Wolfram disease are the combination of the loss of function of *WfS1* and the dominant-negative effect of the mutations. Meta-analysis of genotype–phenotype correlation in Wolfram disease suggested that nonsense or frame-shift mutations caused more severe phenotypes compared with missense mutations (Cano et al., 2007). The *Wfs1* KO mice we analyzed in this study are *Wfs1*-null mice. On the other hand, another line of *Wfs1* KO mice, in which the exon 8 of *Wfs1* is deficient, was reported to show striking behavioral phenotypes (European Patent EP1353549). These findings suggest the possibility that the symptoms of Wolfram disease are accelerated by the aberrant proteins truncated around exon 8. Because function of *Wfs1* has not been well established yet, it is difficult to conclude which mechanism, loss of function or dominant-negative effect, is more influential. Further studies will be necessary to make draw a conclusion.

In summary, we studied the behavior and gene expression patterns in *Wfs1*-null mice. The *Wfs1* KO mice showed several

behavioral features, such as retardation in emotionally triggered motion, decreased social interaction, and enhanced or attenuated behavioral despair depending on experimental conditions. These findings might be relevant to the neuropsychiatric phenotypes reported in patients with Wolfram disease.

Appendix A. Supplementary data

Supplementary data associated with this article can be found, in the online version, at doi:10.1016/j.neures.2008.02.002.

References

Als, T.D., Dahl, H.A., Flint, T.J., Wang, A.G., Vang, M., Mors, O., Kruse, T.A., Ewald, H., 2004. Possible evidence for a common risk locus for bipolar affective disorder and schizophrenia on chromosome 4p16 in patients from the Faroe Islands. Mol. Psychiatry 9, 93–98.

Cano, A., Rouzier, C., Monnot, S., Chabrol, B., Conrath, J., Lecomte, P., Delobel, B., Boileau, P., Valero, R., Procaccio, V., Paquis-Flucklinger, V., Vialettes, B., 2007. Identification of novel mutations in WFS1 and genotype-phenotype correlation in Wolfram syndrome. Am. J. Med. Genet. A 143, 1605–1612.

Cheng, R., Juo, S.H., Loth, J.E., Nee, J., Iossifov, I., Blumenthal, R., Sharpe, L., Kanyas, K., Lerer, B., Lilliston, B., Smith, M., Trautman, K., Gilliam, T.C., Endicott, J., Baron, M., 2006. Genome-wide linkage scan in a large bipolar disorder sample from the National Institute of Mental Health genetics initiative suggests putative loci for bipolar disorder, psychosis, suicide, and panic disorder. Mol. Psychiatry 11, 252–260.

Crawford, J., Zielinski, M.A., Fisher, L.J., Sutherland, G.R., Goldney, R.D., 2002. Is there a relationship between Wolfram syndrome carrier status and suicide? Am. J. Med. Genet. 114, 343–346.

Crawley, J.N., 2007. What's Wrong with My Mouse? Behavioral Phenotyping of Transgenic and Knockout Mice. second ed. Wiley, Hoboken.

Detera-Wadleigh, S.D., Badner, J.A., Berrettini, W.H., Yoshikawa, T., Goldin, L.R., Turner, G., Rollins, D.Y., Moses, T., Sanders, A.R., Karkera, J.D., Esterling, L.E., Zeng, J., Ferraro, T.N., Guroff, J.J., Kazuba, D., Maxwell, M.E., Nurnberger Jr., J.I., Gershon, E.S., 1999. A high-density genome scan detects evidence for a bipolar-disorder susceptibility locus on 13q32 and other potential loci on 1q32 and 18p11.2. Proc. Natl. Acad. Sci. U.S.A. 96, 5604–5609.

Detera-Wadleigh, S.D., Liu, C.Y., Maheshwari, M., Cardona, I., Corona, W., Akula, N., Steele, C.J., Badner, J.A., Kundu, M., Kassem, L., Potash, J.B., Gibbs, R., Gershon, E.S., Mcmahon, F.J., 2007. Sequence variation in DOCK9 and heterogeneity in bipolar disorder. Psychiatry Genet. 17, 274–286.

Domenech, E., Gomez-Zaera, M., Nunes, V., 2006. Wolfram/DIDMOAD syndrome, a heterogenic and molecularly complex neurodegenerative disease. Pediatr. Endocrinol. Rev. 3, 249–257.

Evans, K.L., Lawson, D., Meitinger, T., Blackwood, D.H., Porteous, D.J., 2000. Mutational analysis of the Wolfram syndrome gene in two families with chromosome 4p-linked bipolar affective disorder. Am. J. Med. Genet. 96, 158–160.

Ewald, H., Degn, B., Mors, O., Kruse, T.A., 1998. Support for the possible locus on chromosome 4p16 for bipolar affective disorder. Mol. Psychiatry 3, 442–448.

Ewald, H., Flint, T., Kruse, T.A., Mors, O., 2002. A genome-wide scan shows significant linkage between bipolar disorder and chromosome 12q24.3 and suggestive linkage to chromosomes 1p22-21, 4p16, 6q14-22, 10q26 and 16p13. 3. Mol. Psychiatry 7, 734–744.

File, S.E., Seth, P., 2003. A review of 25 years of the social interaction test. Eur. J. Pharmacol. 463, 35–53.

Fonseca, S.G., Fukuma, M., Lipson, K.L., Nguyen, L.X., Allen, J.R., Oka, Y., Urano, F., 2005. WFS1 is a novel component of the unfolded protein response and maintains homeostasis of the endoplasmic reticulum in pancreatic beta-cells. J. Biol. Chem. 280, 39609–39615.

Gould, T.D., Manji, H.K., 2002. The Wnt signaling pathway in bipolar disorder. Neuroscientist 8, 497–511.

Inoue, H., Tanizawa, Y., Wasson, J., Behn, P., Kalidas, K., Bernal-Mizrachi, E., Mueckler, M., Marshall, H., Donis-Keller, H., Crock, P., Rogers, D., Mikuni, M., Kumashiro, H., Higashi, K., Sobue, G., Oka, Y., Permutt, M.A., 1998. A gene encoding a transmembrane protein is mutated in patients with diabetes mellitus and optic atrophy (Wolfram syndrome). Nat. Genet. 20, 143–148.

Ishihara, H., Takeda, S., Tamura, A., Takahashi, R., Yamaguchi, S., Takei, D., Yamada, T., Inoue, H., Soga, H., Katagiri, H., Tanizawa, Y., Oka, Y., 2004. Disruption of the WFS1 gene in mice causes progressive beta-cell loss and impaired stimulus-secretion coupling in insulin secretion. Hum. Mol. Genet. 13, 1159–1170.

Ishikawa, Y., Katoh, H., Negishi, M., 2006. Small GTPase Rnd1 is involved in neuronal activity-dependent dendritic development in hippocampal neurons. Neurosci. Lett. 400, 218–223.

Joberty, G., Perlungher, R.R., Macara, I.G., 1999. The Borgs, a new family of Cdc42 and TC10 GTPase-interacting proteins. Mol. Cell Biol. 19, 6585–6597.

Kakiuchi, C., Ishiwata, M., Hayashi, A., Kato, T., 2006. XBP1 induces WFS1 through an endoplasmic reticulum stress response element-like motif in SH-SY5Y cells. J. Neurochem. 97, 545–555.

Kasahara, T., Kubota, M., Miyauchi, T., Noda, Y., Mouri, A., Nabeshima, T., Kato, T., 2006. Mice with neuron-specific accumulation of mitochondrial DNA mutations show mood disorder-like phenotypes. Mol. Psychiatry 11, 577–593 523.

Kato, T., Kato, N., 2000. Mitochondrial dysfunction in bipolar disorder. Bipolar Disord. 2, 180–190.

Martorell, L., Zaera, M.G., Valero, J., Serrano, D., Figuera, L., Joven, J., Labad, A., Vilella, E., Nunes, V., 2003. The WFS1 (Wolfram syndrome 1) is not a major susceptibility gene for the development of psychiatric disorders. Psychiatry Genet. 13, 29–32.

Matigian, N., Windus, L., Smith, H., Filippich, C., Pantelis, C., Mcgrath, J., Mowry, B., Hayward, N., 2007. Expression profiling in monozygotic twins discordant for bipolar disorder reveals dysregulation of the WNT signalling pathway. Mol. Psychiatry 12, 815–825.

Miyakawa, T., Leiter, L.M., Gerber, D.J., Gainetdinov, R.R., Sotnikova, T.D., Zeng, H., Caron, M.G., Tonegawa, S., 2003. Conditional calcineurin knockout mice exhibit multiple abnormal behaviors related to schizophrenia. Proc. Natl. Acad. Sci. U.S.A. 100, 8987–8992.

Ohtsuki, T., Ishiguro, H., Yoshikawa, T., Arinami, T., 2000. WFS1 gene mutation search in depressive patients: detection of five missense polymorphisms but no association with depression or bipolar affective disorder. J. Affect Disord. 58, 11–17.

Osman, A.A., Saito, M., Makepeace, C., Permutt, M.A., Schlesinger, P., Mueckler, M., 2003. Wolframin expression induces novel ion channel activity in endoplasmic reticulum membranes and increases intracellular calcium. J. Biol. Chem. 278, 52755–52762.

Overstreet, D.H., Commissaris, R.C., De La Garza 2nd., R., File, S.E., Knapp, D.J., Seiden, L.S., 2003. Involvement of 5-HT1A receptors in animal tests of anxiety and depression: evidence from genetic models. Stress 6, 101–110.

Parra, A., Vinader-Caerols, C., Monleon, S., Simon, V.M., 1999. Learned immobility is also involved in the forced swimming test in mice. Psicothema 11, 239–246.

Philbrook, C., Fritz, E., Weiher, H., 2005. Expressional and functional studies of Wolframin, the gene function deficient in Wolfram syndrome, in mice and patient cells. Exp. Gerontol. 40, 671–678.

Riggs, A.C., Bernal-Mizrachi, E., Ohsugi, M., Wasson, J., Fatrai, S., Welling, C., Murray, J., Schmidt, R.E., Herrera, P.L., Permutt, M.A., 2005. Mice conditionally lacking the Wolfram gene in pancreatic islet beta cells exhibit diabetes as a result of enhanced endoplasmic reticulum stress and apoptosis. Diabetologia 48, 2313–2321.

Rotig, A., Cormier, V., Chatelain, P., Francois, R., Saudubray, J.M., Rustin, P., Munnich, A., 1993. Deletion of mitochondrial DNA in a case of early-onset diabetes mellitus, optic atrophy and deafness (DIDMOAD, Wolfram syndrome). J. Inherit. Metab. Dis. 16, 527–530.

Strom, T.M., Hortnagel, K., Hofmann, S., Gekeler, F., Scharfe, C., Rabl, W., Gerbitz, K.D., Meitinger, T., 1998. Diabetes insipidus, diabetes mellitus,

optic atrophy and deafness (DIDMOAD) caused by mutations in a novel gene (wolframin) coding for a predicted transmembrane protein. Hum. Mol. Genet. 7, 2021–2028.

Swift, M., Swift, R.G., 2000. Psychiatric disorders and mutations at the Wolfram syndrome locus. Biol. Psychiatry 47, 787–793.

Swift, R.G., Sadler, D.B., Swift, M., 1990. Psychiatric findings in Wolfram syndrome homozygotes. Lancet 336, 667–669.

Takeda, K., Inoue, H., Tanizawa, Y., Matsuzaki, Y., Oba, J., Watanabe, Y., Shinoda, K., Oka, Y., 2001. WFS1 (Wolfram syndrome 1) gene product: predominant subcellular localization to endoplasmic reticulum in cultured cells and neuronal expression in rat brain. Hum. Mol. Genet. 10, 477–484.

Takei, D., Ishihara, H., Yamaguchi, S., Yamada, T., Tamura, A., Katagiri, H., Maruyama, Y., Oka, Y., 2006. WFS1 protein modulates the free Ca(2+) concentration in the endoplasmic reticulum. FEBS Lett. 580, 5635–5640.

Threadgill, R., Bobb, K., Ghosh, A., 1997. Regulation of dendritic growth and remodeling by Rho, Rac, and Cdc42. Neuron 19, 625–634.

Torres, R., Leroy, E., Hu, X., Katrivanou, A., Gourzis, P., Papachatzopoulou, A., Athanassiadou, A., Beratis, S., Collier, D., Polymeropoulos, M.H., 2001. Mutation screening of the Wolfram syndrome gene in psychiatric patients. Mol. Psychiatry 6, 39–43.

Yamada, T., Ishihara, H., Tamura, A., Takahashi, R., Yamaguchi, S., Takei, D., Tokita, A., Satake, C., Tashiro, F., Katagiri, H., Aburatani, H., Miyazaki, J., Oka, Y., 2006. WFS1-deficiency increases endoplasmic reticulum stress, impairs cell cycle progression and triggers the apoptotic pathway specifically in pancreatic beta-cells. Hum. Mol. Genet. 15, 1600–1609.

Dual involvement of G-substrate in motor learning revealed by gene deletion

Shogo Endo[a,1], Fumihiro Shutoh[b,1], Tung Le Dinh[c,1], Takehito Okamoto[b], Toshio Ikeda[d], Michiyuki Suzuki[e], Shigenori Kawahara[e], Dai Yanagihara[f], Yamato Sato[f], Kazuyuki Yamada[g], Toshiro Sakamoto[a], Yutaka Kirino[e], Nicholas A. Hartell[h], Kazuhiko Yamaguchi[c], Shigeyoshi Itohara[d], Angus C. Nairn[i], Paul Greengard[j], Soichi Nagao[b], and Masao Ito[c,2]

[a]Unit for Molecular Neurobiology of Learning and Memory, Okinawa Institute of Science and Technology, Uruma 904-2234, Japan; [b]Laboratory for Motor Learning Control, [c]Laboratory for Memory and Learning, [d]Laboratory for Behavioral Genetics, and [g]Support Unit for Animal Experiment, Research Resources Center, RIKEN Brain Science Institute, Wako 351-0198, Japan; [e]Laboratory for Neurobiophysics, School of Pharmaceutical Sciences, University of Tokyo, Tokyo 113-0033, Japan; [f]Department of Life Sciences, Graduate School of Arts and Sciences, University of Tokyo, Tokyo 153-8902, Japan; [h]Department of Cell Physiology and Pharmacology, University of Leicester, Leicester LE1 9HN, United Kingdom; [i]Department of Psychiatry, Yale University School of Medicine, New Haven, CT 06519; and [j]Laboratory for Molecular and Cellular Neuroscience, The Rockefeller University, New York, NY 10021-6399

Contributed by Masao Ito, December 30, 2008 (sent for review December 7, 2008)

In this study, we generated mice lacking the gene for G-substrate, a specific substrate for cGMP-dependent protein kinase uniquely located in cerebellar Purkinje cells, and explored their specific functional deficits. G-substrate–deficient Purkinje cells in slices obtained at postnatal weeks (PWs) 10–15 maintained electrophysiological properties essentially similar to those from WT littermates. Conjunction of parallel fiber stimulation and depolarizing pulses induced long-term depression (LTD) normally. At younger ages, however, LTD attenuated temporarily at PW6 and recovered thereafter. In parallel with LTD, short-term (1 h) adaptation of optokinetic eye movement response (OKR) temporarily diminished at PW6. Young adult G-substrate knockout mice tested at PW12 exhibited no significant differences from their WT littermates in terms of brain structure, general behavior, locomotor behavior on a rotor rod or treadmill, eyeblink conditioning, dynamic characteristics of OKR, or short-term OKR adaptation. One unique change detected was a modest but significant attenuation in the long-term (5 days) adaptation of OKR. The present results support the concept that LTD is causal to short-term adaptation and reveal the dual functional involvement of G-substrate in neuronal mechanisms of the cerebellum for both short-term and long-term adaptation.

cerebellum | long-term depression | optokinetic response | Purkinje cell

The G-substrate purified from rabbit cerebellum is one of the few preferred substrates for cGMP-dependent protein kinase (PKG) (1–8). It is positioned at the downstream end of the cascade linking nitric oxide (NO), soluble guanylate cyclase, cGMP, and PKG. The target(s) for NO is located within Purkinje cells (9–12), where diffusing NO activates soluble guanylate cyclase (13), which, in turn, enhances PKG activity (14). Immunohistochemical studies have revealed that G-substrate is uniquely concentrated in cerebellar Purkinje cells (2, 6, 7, 15, 16). In cerebellar slices, G-substrate in Purkinje cells is effectively phosphorylated in response to a membrane-permeable analogue of cGMP that activates PKG (9). Phosphorylated G-substrate acts as a potent inhibitor of protein phosphatase (PP) 1 and PP2A (6–8). We now have generated G-substrate knockout mice to investigate further the functional roles of G-substrate at cellular and behavioral levels.

Each component of the NO-cGMP-PKG pathway has so far been shown to be required for the induction of cerebellar long-term depression (LTD) (12, 17–24), a characteristic form of synaptic plasticity displayed by Purkinje cells (25). In LTD, synaptic transmission from parallel fibers (PFs) to Purkinje cells is persistently depressed after conjunctive stimulation of the PFs and climbing fibers (CFs). CF stimuli can be replaced by application of depolarizing pulses to the Purkinje cell membrane. Peculiarly, NO is not required for LTD induction in young cultured Purkinje cells (26), suggesting that the NO-cGMP-PKG pathway acts as a modulator whose requirement for LTD may depend on various circumstances (27).

LTD has been considered to provide a cellular mechanism of motor learning (25). Here, we report a distinctive age-dependent deficit of LTD induction in G-substrate–deficient Purkinje cells; LTD occurs at postnatal week (PW) 4 but diminishes at PW5–6 and then recovers at PW10 afterward. We also examined how the age-dependent diminution of LTD is reflected in the age profile of adaptation of optokinetic eye movement response (OKR), a simple form of motor learning. OKR adaptation is an increase of OKR gain induced by continuous oscillation of a screen around a stationary animal and is abolished by gene knockout (28) or pharmacological inhibition of neural NOS (28, 29). As very recently reported, OKR adaptation (30), as well as vestibulo-ocular reflex (VOR) adaptation (31), has 2 distinct phases underlain by different neural mechanisms. The short-term adaptation occurring during 1 h of training has its memory site in the cerebellar cortex of the flocculus, whereas the long-term adaptation accumulated during repeated 5-day training sessions is an event that takes place somewhere else, because the latter is maintained even after a glutamate antagonist (31) or lidocaine (30) has blocked cerebellar cortical activity. There is some evidence indicating that long-term OKR adaptation has its memory site in vestibular nuclear neurons (30).

In this study, we demonstrate in G-substrate knockout mice that the short-term OKR adaptation diminishes in an age-dependent manner in parallel with LTD amplitude reduction. G-substrate knockout affects the LTD induction and short-term OKR adaptation only temporarily around PW6; however, young adult mice at PW12 prove to be free of these deficits. We demonstrate that they are also free of deficits in other motor learning tasks, including eyeblink conditioning (32), motor coordination (33), and adaptive locomotion (34). Eventually, a significant depression of the long-term OKR adaptation is the only deficit exhibited by PW12 G-substrate knockout mice. Thus, the functional role of G-substrate gene is defined by its differential involvement in LTD-driven short-term OKR adaptation and otherwise initiated long-term OKR adaptation.

Author contributions: S.E., F.S., T.L.D., T.I., S.K., D.Y., Y.S., K. Yamada, Y.K., S.I., A.C.N., P.G., S.N., and M.I. designed research; S.E., F.S., T.L.D., T.O., T.I., M.S., S.K., D.Y., Y.S., K. Yamada, N.A.H., and K. Yamaguchi performed research; S.E., F.S., T.L.D., T.O., D.Y., Y.S., T.S., N.A.H., K. Yamaguchi, S.N., and M.I. analyzed data; and S.E. and M.I. wrote the paper.

The authors declare no conflict of interest.

Freely available online through the PNAS open access option.

[1]S.E., F.S., and T.L.D. contributed equally to this work.

[2]To whom correspondence should be addressed. E-mail: masao@brain.riken.jp.

This article contains supporting information online at www.pnas.org/cgi/content/full/0813341106/DCSupplemental.

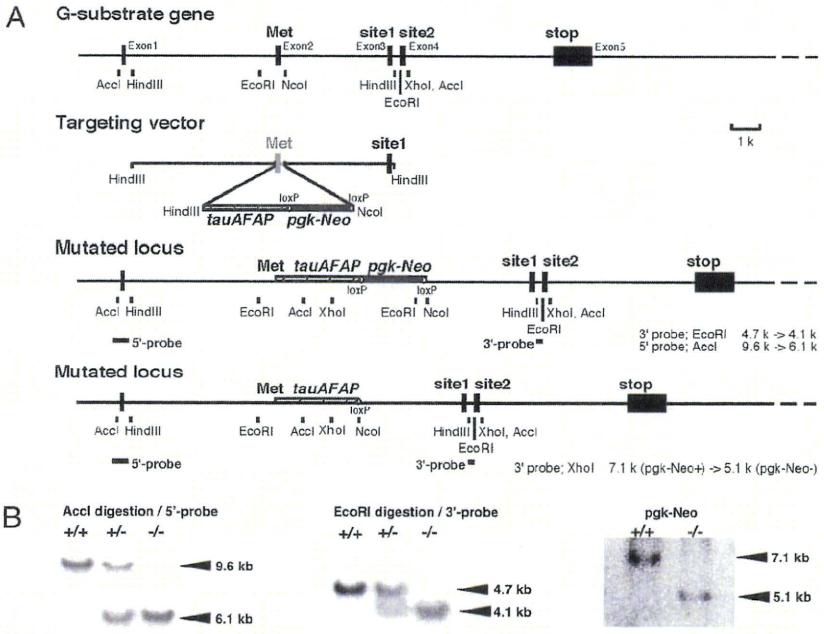

Fig. 1. Generation of G-substrate knockout mice. (*A*) Gene structure of mouse G-substrate and targeting vector for the generation of G-substrate knockout mice. (*B*) Confirmation of G-substrate knockout by Southern blot analysis. Restriction-enzyme–digested genomic DNA was subjected to Southern blot hybridization analysis. The band shift attributable to the homologous recombination was confirmed by probing the blot with ^{32}P-labeled 3′- and 5′-probes, as indicated in the figure. The removal of the selection marker, pgk-Neo cassette, was also confirmed by Southern blot analysis using the ^{32}P-labeled 3′-probe.

Results

Generation of G-Substrate Knockout Mice. The G-substrate gene consists of 5 exons and 4 introns (Fig. 1*A*). The initiation Met is in exon 2, and the 2 PKG phosphorylation sites are in separate exons (exons 3 and 4). For the generation of G-substrate knockout mice, the G-substrate gene was disrupted by insertion of DNA encoding a selection marker (pgk-neo cassette) and tau-AFAP in the first coding exon (exon 2) (Fig. 1*A*). Correct recombination was confirmed by Southern blot analysis of ES cells and F2 mice using 5′- and 3′-probes (Fig. 1*B*). The removal of the pgk-neo cassette, the selection marker in ES cells, was confirmed by Southern blot analysis (Fig. 1*B*). Homozygous mice deficient in G-substrate were obtained by mating heterozygous mice and had normal Mendelian distribution, showing lack of embryonic lethality. The homozygous G-substrate knockout mice appeared to develop and reproduce normally.

In samples from WT mice, mRNA was observed as a single band of 1.7 kb on Northern blot analysis; however, there was complete absence of G-substrate mRNA and immunoreactivity in the homozygous knockout mice [supporting information (SI) Fig. S1*A* and *B*]. Furthermore, no detectable G-substrate protein was observed in homogenates prepared from G-substrate knockout mice as demonstrated by immunoblotting of immunoprecipitates obtained using G-substrate antibody (Fig. S1*C*).

The results suggest that the homozygous G-substrate gene deletion led to a complete loss of the G-substrate mRNA and protein expression in the cerebellum. No major morphological changes were observed in the cerebellum or whole brain of homozygote mice as assessed by light microscopy (Fig. 2 *A* and *B*). The layer structures of the cerebellum were indistinguishable in WT and G-substrate knockout mice, as shown by Nissl staining of cerebellar slices. There were no apparent changes in the density, size, or shape of cerebellar Purkinje cells. In G-substrate knockout mice, the shape and path of Purkinje cells were easily visualized by fluorescence microscopy (Fig. 2*C*), given that AFAP, a GFP derivative, was expressed in G-substrate knockout mice under the control of the G-substrate promoter (Fig. 1). Primary and secondary dendrites and axon bundles were observed with bright fluorescence. Furthermore, axon bundles originating from Purkinje cells were clearly marked by AFAP. These axons course to the deep cerebellar nucleus and vestibular nucleus, as in normal mice.

Cerebellar LTD. In current clamp configuration with patch pipettes, we recorded from 120 Purkinje cells in acute slices from G-substrate knockout mice and from 118 Purkinje cells in acute slices from WT littermates. We confirmed that there were no statistically significant differences in membrane potential, membrane resistance, time course of PF-evoked excitatory postsynaptic potentials (EPSP), or waveform of complex spikes, except for a modest difference in paired-pulse facilitation of PF-EPSPs (Table S1). Stimulation of the white matter evoked full-sized CF responses in an all-or-none manner, and there was no evidence for multiple CF innervations of Purkinje cells.

Cerebellar LTD was induced by conjunction of PF stimulation with depolarizing pulses at 1 Hz for 5 min (see *Materials and Methods*). The induced LTD developed during the initial 20 min and was followed by a slow phase proceeding for another 40 min (Fig. 3*A*). Because our provisional tests showed variation in the expression of LTD in Purkinje cells deficient of G-substrate, we paid special attention to the possible age-dependent variation of LTD and examined mice at PW4 to PW15. As shown in Fig. 3*A*, WT Purkinje cells showed virtually identical average LTD time courses throughout life up to PW15. The magnitudes of LTD measured 41–50 min after the onset of 5 min of conjunction were about 20%, on average (Fig. 3*A*). In contrast, Purkinje cells lacking G-substrate showed virtually normal LTD at PW4, which then diminished to zero at PW6; thereafter it recovered to normal levels from PW10 onward (Fig. 3*B*). The histogram in Fig. 3*C* compares the LTD magnitude between G-substrate–deficient and WT Purkinje cells from PW4 to PW15. There was a significant difference in the LTD magnitude between the 2

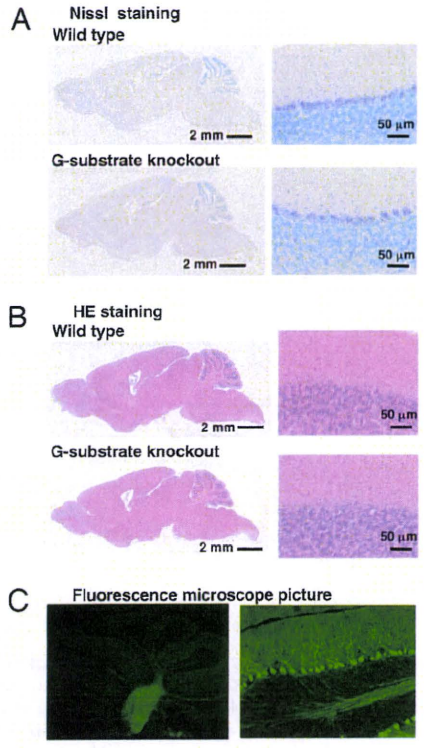

Fig. 2. Structures of cerebellum in WT and G-substrate knockout mice. (*A*) Nissl staining of cerebellar slices obtained from WT and G-substrate knockout mice. The thin sections (30 μm) were obtained from paraformaldehyde-fixed brain using a cryostat and were subjected to Nissl staining. (*B*) Hematoxylin and Eosin staining of brain slices obtained from WT and G-substrate knockout mice. (*C*) Fluorescence images of slices obtained from G-substrate knockout mice. The frozen thin sections (20 μm) were observed under a fluorescence microscope. AFAP, a GFP derivative, was expressed under the control of the G-substrate promoter.

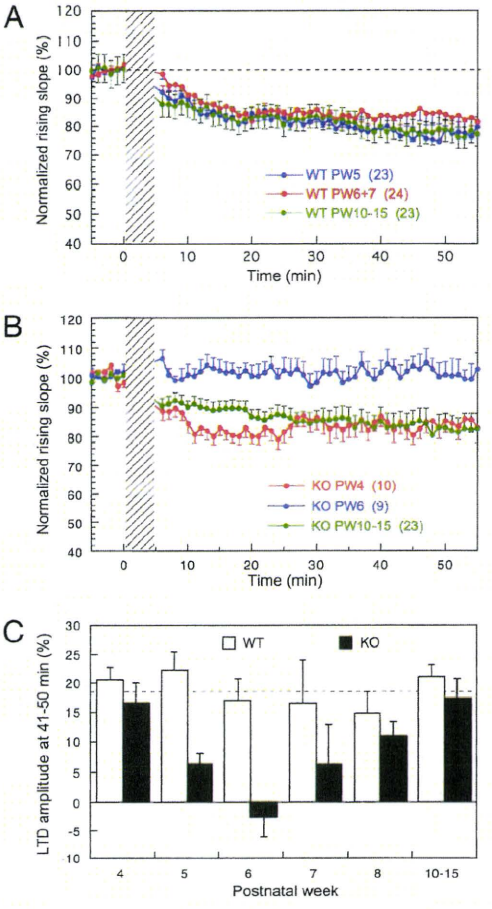

Fig. 3. Age-dependent expression of cerebellar LTD in G-substrate–lacking Purkinje cells. (*A*) Averaged time profile of 3 groups of WT Purkinje cells is shown with different colors. The ordinate illustrates the rising slope of PF-EPSPs relative to the average measured 5 min before conjunction, and the abscissa illustrates time. The oblique-shaded band indicates the application of conjunction of PF stimulation and depolarizing pulses. Number of Purkinje cells tested is shown in brackets. Vertical bars, SEs. (*B*) Similar to *A* but for G-substrate–deficient Purkinje cells. (*C*) Histograms showing LTD amplitude at 41–50 min for different PWs in WT and G-substrate–deficient Purkinje cells. Filled columns are G-substrate knockout mice, and empty columns are WT littermates. Vertical bars, SEs. The numbers of cells used for the experiments are as follows: for WT mice, PW4 (12), PW5 (23), PW6 (14), PW7 (10), PW8 (14), and PW10–15 (23); for G-substrate knockout mice, PW4 (10), PW5 (9), PW6 (9), PW7 (6), PW8 (11), and PW10–15 (29).

genotypes of Purkinje cells (2-way factorial ANOVA: $F_{1,\ 158} = 13.19, P = 0.004$). The LTD magnitude in G-substrate knockout mice showed a clear age-dependency (1-way ANOVA: $F_{5,\ 68} = 2.91, P = 0.019$), whereas the incidence and extent of LTD in WT mice did not ($F_{5,\ 90} = 0.671, P = 0.647$). The Dunnett post hoc test in Fig. 3*C* revealed that the LTD magnitude in G-substrate knockout Purkinje cells was significantly smaller than that in WT Purkinje cells at PW6 ($P < 0.01$) and PW5 ($P < 0.05$). LTD magnitudes in G-substrate knockout mice were also smaller at PW7 and PW8 (Fig. 3*C*), but these decreases were not statistically significant ($P > 0.05$).

Dynamics and Short-Term Adaptation of OKR. First, we examined the dynamic characteristics of the OKR (gain, phase, and screen frequency dependence) using sinusoidal screen oscillations (15° peak-to-peak, 0.11–0.33 Hz) in the light in 9 G-substrate knockout mice and 7 WT littermate mice at PW12 (Fig. S2). We observed no differences in the gains of OKR between G-substrate knockout and WT littermates (two-way repeated measures ANOVA: $F_{1,\ 14} = 0.082, P = 0.78$). Then, we examined the adaptation of OKR in 12 G-substrate knockout mice and 12 WT littermates at PW12. As shown in Fig. *4A*, no difference was observed in the "start gain" of OKR measured by sinusoidal screen oscillation (15° peak-to-peak, 0.17 Hz, maximum screen velocity of 7.9°/sec) between the 2 genotypes at PW12. These mice were subjected to 1-hr continuous screen oscillation with the same stimulus parameters to induce short-term OKR adaptation. The "end gain" of OKR was measured immediately after the 1-hr screen oscillation. The increase in the OKR gain during the 1-hr screen oscillation ([end gain] − [start gain]) represents the magnitude of the short-term OKR adaptation. As shown in Fig. *4B*, no significant difference was detected in short-term OKR adaptation in G-substrate knockout mice and WT littermates at PW12 [Student's *t* test: $t\ (22) = 0.26, P = 0.797$].

We also examined 14 G-substrate knockout mice and 10 WT mice at PW6 (all different from the mice examined previously at PW12). Fig *4C* shows that there was no significant difference in the start OKR gain between the 2 genotypes at PW6. However, a significant difference was detected in the short-term OKR adaptation between the 2 genotypes at PW6 (Fig. 4*D*); the magnitude of short-term OKR adaptation was smaller in G-substrate knockout mice than in WT mice [Student's *t* test: $t\ (22) = 2.094, P = 0.048$]. Furthermore, examination of the mice at PW4 and PW5 revealed a low OKR gain and poor short-term OKR adaptation for both G-substrate knockout and WT litter-

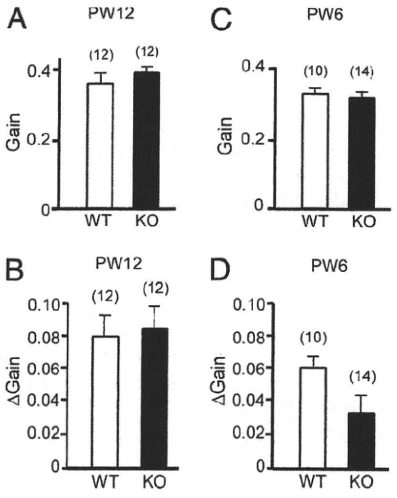

Fig. 4. OKR gain and short-term OKR adaptation. Mice were subjected to sinusoidal screen oscillation by 15° (peak-to-peak) at 0.17 Hz (maximum velocity, 7.9°/sec) in the light for 1 hr. (*A*) Start OKR gain before 1-hr screen oscillation at PW12. (*B*) OKR gain change obtained during 1-hr sustained screen oscillation at PW12. (*C*) Similar to *A* but at PW6. (*D*) Similar to *B* but at PW6. Filled columns represent G-substrate knockout (KO) mice, and empty columns represent WT mice. Vertical bars, SEs. The number of mice used is shown in brackets.

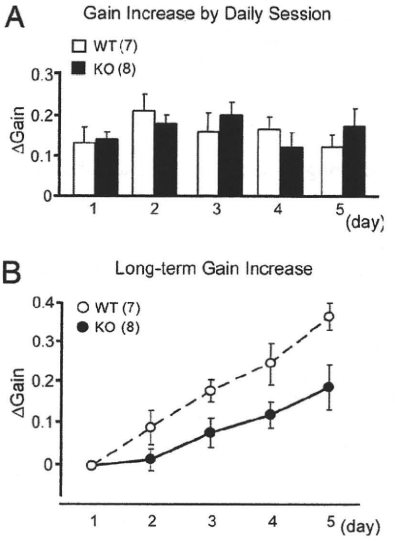

Fig. 5. Long-term adaptation of OKR. WT ($n = 7$) and G-substrate knockout (KO) mice ($n = 8$) at PW12–15 were exposed to 1-hr sustained screen oscillation every day for 5 days. The mice were kept in the dark, except during the screen oscillation. (*A*) Daily OKR adaptation. The ordinate illustrates ΔGain, gain changes obtained after 1-hr oscillation on each day. Filled columns are G-substrate KO mice, and empty columns are WT littermates. (*B*) Cumulative OKR gain changes induced through 5-day sessions. The ordinate illustrates ΔGain, increases of the start gains on each day as measured from the start gain at day 1. Hollow circles represent WT mice, and solid circles represent G-substrate KO mice.

mates (data not shown). It appears that the OKR neuronal circuit is immature at PW4 and PW5, such that short-term OKR adaptation occurs only rudimentarily. The results in Fig. 4 *B* and *D* suggest that the OKR neuronal circuit has matured considerably by PW6, although it might not be as complete as that at PW12, and that it expresses a deficit caused by G-substrate knockout. These interpretations are consistent with the results shown in Fig. 3*C* (i.e., LTD attenuates at PW6 but recovers at PW12).

Long-Term OKR Adaptation. Next, we examined long-term OKR adaptation by carrying out 1 session of 1-hr screen oscillation per day for 5 successive days. Fig. 5*A* shows that the daily gain changes ([end gain] − [start gain]) did not show significant differences between the WT and G-substrate knockout mice throughout 5 days (two-way repeated measures ANOVA: $F_{1, 13} = 0.019, P = 0.893$). The increase in the daily gain recovered within 24 hr; however, the start gain before the 1-hr oscillation gradually increased at days 2–5 compared with the start gain at day 1, which we call long-term adaptation (30). Fig. 5*B* compares the gain increase induced by long-term OKR adaptation between the 2 genotypes. The gain increase of the G-substrate knockout mice was smaller than that of the WT mice throughout the 5-day session (two-way repeated measures ANOVA: $F_{1, 13} = 6.508, P = 0.024$) (Fig. 5*B*). At the end of day 5, the start gain increased by 0.19 in G-substrate knockout mice, whereas it increased by 0.37 in the WT mice (Fig. 5*B*). Thus, G-substrate knockout mice are characterized by a partial but significant decrease in the rate of long-term OKR adaptation. The long-term OKR adaptation is not an accumulation of residuals of short-term adaptation, because the former remained intact with local application of lidocaine to the flocculus (30), which blocks the latter. The present results showing that, at PW12, long-term OKR adaptation attenuates, whereas short-term OKR adaptation occurs normally provide another line of evidence that the 2 types of OKR adaptation are underlain by different neural mechanisms.

General Behavior. Behavioral tests described in this article were carried out on young adult mice at PW12, unless otherwise stated. The overall behavioral properties of G-substrate knockout mice were not different from those of WT mice (summarized in Table S2). G-substrate knockout mice exhibited some decrease in locomotor activity in the open-field test; however, the data did not reach statistical significance, except for the distance moved in the dark condition (Fig. S3). The decreased distance moved in the open field might imply an emotional change in G-substrate knockout mice. However, we confirmed that G-substrate knockout mice have normal sensory systems, and they behaved normally in a variety of other emotional tests carried out in the entire test battery (Table S2). A further detailed analysis is required to identify the possible emotional change implied by the open-field test results.

Rotor Rod Test and Gait Analyses. Motor coordination was examined in the G-substrate knockout and WT mice using the rotor rod test at a speed of 8 rotations per min (rpm) (Fig. S4*A*) and 12 rpm (data not shown). G-substrate knockout mice and WT mice indistinguishably improved their retention time before falling during repeated trials (two-way repeated measures ANOVA: $F_{1, 9} = 0.015$, $P = 0.907$). Furthermore, the results obtained 24 hr after the initial 10 trials at 8 rpm were not different between WT and G-substrate knockout mice (data not shown).

We examined the kinematics of gait using high-speed video recordings during treadmill locomotion to characterize locomotor movements. No significant differences were observed between WT and G-substrate knockout mice in terms of temporal parameters such as step cycle duration, swing phase duration, stance phase duration, and bisupport phase duration (Table S3). As the treadmill speed increased, the step cycle duration and stance phase duration decreased, although the swing phase duration remained nearly constant in both lines of mice. The angular excursions of the knee and ankle were similar in the WT and knockout mice, although the joints stayed in slightly ex-

tended positions in G-substrate knockout mice (Fig. S4 *B* and *C*). G-substrate knockout mice did not show any appreciable abnormality in motor coordination and hind limb kinematics during treadmill locomotion, and it is concluded that the gait in G-substrate knockout mice is not ataxic.

Eyeblink Conditioning. This is a well-established form of cerebellum-dependent motor learning (35), and some genetically modified mouse lines with impaired cerebellar LTD have been reported to show abnormality in eyeblink conditioning (36–40). In this study, G-substrate knockout mice acquired the task as quickly as the WT mice in delay eyeblink conditioning tasks (Fig. S5*A*) and in trace eyeblink conditioning tasks (Fig. S5*B*).

Discussion

Homozygotic G-substrate–deficient mice survived and were normal in terms of morphology of the cerebellum (Fig. 2) and other brain areas, general behaviors (Table S1 and Figs. S2 and S3), and reproduction. G-substrate knockout mice thus share a disturbance-free phenotype with Purkinje cell-specific (PKGI) knockout mice (24). This is partly because both PKG and G-substrate are localized in Purkinje cells, but it is also because the deletion of PKGI (24) or G-substrate (see *Results*) does not cause multiple innervations of Purkinje cells by CFs, which may lead to ataxia or seizure.

The temporary hiatus of LTD and short-term OKR adaptation in G-substrate knockout mice around PW6 may suggest that the NO-cGMP-PKG-G-substrate pathway becomes essential during this crucial stage of development. At other times, it plays an accessory role rather than an essential role. At the end of this pathway, PKG-phosphorylated G-substrate acts as a potent inhibitor of PP1 and PP2A (6–8). Complex involvement of PPs in cerebellar LTD has been observed in cultured Purkinje cells; myosin/moesin phosphatase (containing PP1 catalytic subunit in its complex) plays a major role at 9–16 days in vitro (DIV) (41), but at 22–35 DIV, PP2A takes over (42). Hence, it is possible that, underlying the age profile of LTD (Fig. 3*C*), G-substrate comes into play as a preferential inhibitor of PP2A with a delay of 6 weeks, and then is probably replaced by PW10 with another PP inhibitor, which is currently unknown. The results indicating that G-substrate knockout attenuates both cerebellar LTD and short-term OKR adaptation temporarily at the early stage of development (Figs. 3*C* and 4*D*) conform to previous results showing that blockade of LTD leads to impairment of short-term OKR adaptation (28). Together, these results consistently support the current view that LTD is an essential mechanism of cerebellum-dependent learning. In this context, a close association was also reported very recently in mice lacking delphilin in Purkinje cells, whose LTD induction and OKR adaptation were both enhanced (43). Temporary diminution of LTD, which is now shown to be associated with attenuation of short-term OKR adaptation in G-substrate knockout mice, may also impair other forms of motor learning such as motor coordination on the rotor rod and eyeblink conditioning. We leave analyses of this association to future study until the dual-phase mechanism, which is the basis of the present analysis of OKR adaptation, is also defined for other forms of motor learning.

In G-substrate knockout mice at PW12, LTD induction and short-term OKR adaptation occurred normally (Figs. 3*A* and 4*B*) but long-term adaptation was significantly impaired (Fig. 5*B*). This long-term adaptation is caused by a slowly developed potentiation of synaptic transmission or an intrinsic excitability in vestibular relay neurons (30). The partial impairment of long-term VOR adaptation was also reported to occur in Purkinje cell-specific PKGI-deficient mice with normal short-term adaptation (24). Therefore, the NO-cGMP-PKG-G-substrate cascade appears to play an essential role in the induction of long-term VOR and OKR adaptations, which cannot be compensated for by another pathway. Long-term VOR and OKR adaptations would share a common synaptic mechanism at vestibular relay neurons (44). How the lack of G-substrate in Purkinje cells impairs the adaptive mechanism in vestibular relay neurons is presently unknown. Preliminary results suggest that G-substrate undergoes intracellular translocation from the cell nucleus to cytosol in response to the membrane-permeable analogue of cGMP, 8-bromoguanosine 3′: 5′-cyclic monophosphate (M.S. and S.E., unpublished observation). Recently, the DARPP-32, a PP inhibitor in striatal neurons, was reported to translocate to the cell nuclei, and the translocation was associated with increased histone H3 phosphorylation, an important component of nucleosomal response such as transcription (45). G-substrate translocation may lead to changes in the state of protein phosphorylation in the nucleus and cytosol, or it may affect transcription-translation systems. These effects potentially affect molecular events in the axon terminals of Purkinje cells, which would, in turn, act on vestibular relay neurons transsynaptically.

Conclusion

We have shown that G-substrate knockout causes dual deficits in motor learning. It attenuates cerebellar LTD and associated short-term adaptation temporarily at the early stage of development, consistent with the current view that LTD is an essential mechanism of cerebellum-dependent learning, and it also persistently impairs long-term adaptation of OKR. Otherwise, the G-substrate knockout mice are surprisingly free of disturbances in neuronal functions or behaviors. These mice provide a good model for the investigation of cellular, molecular, and genetic mechanisms underlying the short-term and long-term adaptations of motor behaviors.

Materials and Methods

Isolation and Targeted Disruption of Mouse G-Substrate Gene. The cDNA for mouse G-substrate was obtained from mouse cerebellum by PCR using the primer sets based on human (6) and rat (7) G-substrate cDNA. Then, a mouse C57BL/6 genomic library (46) constructed in a BAC plasmid was screened using a random-primed cDNA probe for mouse G-substrate. Positive clones were analyzed by restriction mapping and sequencing using a GPS system (NEB).

The standard technique for gene targeting (47) was used. Targeting vectors were constructed in pBluescript to replace exon 2 of the G-substrate gene, which encodes the initiation site Met, with the tau-AFAP-pgk-Neo cassette (Fig. 1). Detailed methods for confirmation of positive clones and generation of chimeric mice and mice harboring the knockout allele are provided in *SI Text* and in Fig. 1. Total RNA was isolated from the cerebellum using Sepasol (Nakalai Tesque) and was analyzed by Northern blotting analysis using a ^{32}P-labeled mouse G-substrate probe (corresponding to nucleotides 129–608 of AF071562). The blots were hybridized in QuikHyb hybridization solution (Stratagene) at 65 °C overnight and washed with 0.2× SSC containing 0.1% SDS. The hybridization signals on the blots were analyzed using a phosphorimager BAS5000 (Fuji Film).

Immunohistochemistry. Paraformaldehyde-fixed brain slices were stained with affinity-purified anti-G-substrate antibodies (7). Immunoreaction was visualized with Alexa Fluor 546-conjugated anti-mouse IgG (Molecular Probes). Fluorescent image stainings were obtained using an FX1000 confocal fluorescence microscope (Olympus).

Immunoprecipitation and Immunoblots. Mouse cerebella were homogenized in extraction buffer containing 50 mM Tris-HCl (pH 7.5), protease inhibitor mixture (Roche Diagnostics), 25 mM β-glycerophosphate, and 1% Nonidet P-40. The homogenates were centrifuged at 100,000 × *g* for 1 h, and the resulting supernatants were then subjected to immunoprecipitation. Affinity-purified rabbit anti-G-substrate antibodies against the amino terminus portion or the carboxyl terminus portion of G-substrate were used for the immunoprecipitation (7). Immunoprecipitates were subjected to SDS/PAGE, followed by immunoblot analysis. The protein concentration was determined by the method of Bradford (48) using BSA as the standard.

Slice Experiments. Under general anesthesia by ether inhalation, mice were decapitated and the cerebellum was excised. Sagittal slices of 300 μm thickness were prepared from the vermis. The recording chamber was perfused with oxygenated Ringer's solution containing 100 μM picrotoxin at 30–31 °C. Under an upright microscope, whole-cell patch-clamp recordings were performed using borosilicate pipettes (resistance, 3–5 MΩ). A Multiclamp700A amplifier (Axon) and pClamp 9 software (Axon) were used. PFs were focally stimulated through a glass pipette. To induce LTD, depolarizing pulses of 200 msec duration were applied to Purkinje cell membrane and adjusted (within 2 nA) to evoke at least 1 Ca^{2+} spike. PFs were stimulated with double pulses (each 0.1 msec in duration) paired at 50-msec intervals timed in such a way that the first pulse fell 30 msec later than the onset of each depolarizing pulse. The combination of double PF stimuli and a depolarizing pulse was repeated at 1 Hz for 5 min (300 pulses) in each trial of LTD induction.

Behavioral Analysis. For this purpose, mice were backcrossed with C57BL/6 for at least 5 generations. Protocols for all animal experiments were approved by the animal experiment committees of the RIKEN Brain Science Institute, Okinawa Institute of Science and Technology, and the other authors' institutions. Maximum efforts were made to reduce the stress of the mice. Detailed methods for the behavioral analyses, including general behaviors, eye movement, eyeblink conditioning, and rotor rod and treadmill locomotion, are provided in *SI Text*.

ACKNOWLEDGMENTS. We thank Ms. Masako Suzuki for the generation of G-substrate knockout mice and Dr. Mariko Sumi and Ms. Yumiko Motoyama for other technical assistance. MS12 cells were a generous gift from the Meiji Dairies Corporation. This work was supported by a grant for collaboration of the Okinawa Institute of Science and Technology and RIKEN Brain Science Institute and by grants from Ministry of Education, Culture, Sports, Science, and Technology of Japan.

1. Schlichter DJ, Casnellie JE, Greengard P (1978) An endogenous substrate for cGMP-dependent protein kinase in mammalian cerebellum. *Nature* 273:61–62.
2. Schlichter DJ, *et al.* (1980) Localization of cyclic GMP-dependent protein kinase and substrate in mammalian cerebellum. *Proc Natl Acad Sci USA* 77:5537–5541.
3. Aswad DW, Greengard P (1981) A specific substrate from rabbit cerebellum for guanosine 3′:5′-monophosphate-dependent protein kinase. I. Purification and characterization. *J Biol Chem* 256:3487–3493.
4. Aswad DW, Greengard P (1981) A specific substrate from rabbit cerebellum for guanosine 3′:5′-monophosphate-dependent protein kinase. II. Kinetic studies on its phosphorylation by guanosine 3′:5′-monophosphate-dependent and adenosine 3′:5′-monophosphate-dependent protein kinases. *J Biol Chem* 256:3494–3500.
5. Aitken A, *et al.* (1981) A specific substrate from rabbit cerebellum for guanosine-3′:5′-monophosphate-dependent protein kinase. III. Amino acid sequences at the two phosphorylation sites. *J Biol Chem* 256:3501–3506.
6. Endo S, *et al.* (1999) Molecular identification of human G-substrate, a possible downstream component of the cGMP-dependent protein kinase cascade in cerebellar Purkinje cells. *Proc Natl Acad Sci USA* 96:2467–2472.
7. Endo S, Nairn AC, Greengard P, Ito M (2003) Thr123 of rat G-substrate contributes to its action as a protein phosphatase inhibitor. *Neurosci Res (NY)* 45:79–89.
8. Hall KU, *et al.* (1999) Phosphorylation-dependent inhibition of protein phosphatase-1 by G-substrate. A Purkinje cell substrate of the cyclic GMP-dependent protein kinase. *J Biol Chem* 274:3485–3495.
9. Hartell NA (1994) cGMP acts within cerebellar Purkinje cells to produce long term depression via mechanisms involving PKC and PKG. *NeuroReport* 5:833–836.
10. Lev-Ram V, *et al.* (1995) Long-term depression in cerebellar Purkinje neurons results from coincidence of nitric oxide and depolarization-induced Ca^{2+} transients. *Neuron* 15:407–415.
11. Lev-Ram V, *et al.* (1997) Synergies and coincidence requirements between NO, cGMP, and Ca^{2+} in the induction of cerebellar long-term depression. *Neuron* 18:1025–1038.
12. Shin JH, Linden DJ (2005) An NMDA receptor/nitric oxide cascade is involved in cerebellar LTD but is not localized to the parallel fiber terminal. *J Neurophysiol* 94:4281–4289.
13. Stone JR, Marlette MA (1996) Soluble guanylate cyclase from bovine lung: Activation with nitric oxide and carbon monoxide and spectral characterization of the ferrous and ferric states. *Biochemistry* 35:1094–1099.
14. Hartell NA, Furuya S, Jacoby S, Okada D (2001) Intercellular action of nitric oxide increases cGMP in cerebellar Purkinje cells. *NeuroReport* 12:25–28.
15. Detre JA, Nairn AC, Aswad DW, Greengard P (1984) Localization in mammalian brain of G-substrate, a specific substrate for guanosine 3′, 5′-cyclic monophosphate-dependent protein kinase. *J Neurosci* 4:2843–2849.
16. Qian Y, *et al.* (1996) cGMP-dependent protein kinase in dorsal root ganglion: Relationship with nitric oxide synthase and nociceptive neurons. *J Neurosci* 16:3130–3138.
17. Crepel F, Jaillard D (1990) Protein kinases, nitric oxide and long-term depression of synapses in the cerebellum. *NeuroReport* 1:122–136.
18. Ito M, Karachot L (1990) Messengers mediating long-term desensitization in cerebellar Purkinje cells. *NeuroReport* 1:129–132.
19. Shibuki K, Okada D (1991) Endogenous nitric oxide release required for long-term synaptic depression in the cerebellum. *Nature* 349:326–328.
20. Daniel H, Hemart N, Jaillard D, Crepel F (1993) Long-term depression requires nitric oxide and guanosine 3′:5′ cyclic monophosphate production in rat cerebellar Purkinje cells. *Eur J Neurosci* 5:1079–1082.
21. Lev-Ram V, *et al.* (1997) Absence of cerebellar long-term depression in mice lacking neuronal nitric oxide synthase. *Learn Mem* 4:169–717.
22. Boxall AR, Garthwaite J (1996) Long-term depression in rat cerebellum requires both NO synthase and NO-sensitive guanylyl cyclase. *Eur J Neurosci* 8:2209–2212.
23. Jacoby S, Sims RE, Hartell NA (2001) Nitric oxide is required for the induction and heterosynaptic spread of cerebellar LTP. *J Physiol (London)* 535:825–839.
24. Feil R, *et al.* (2003) Impairment of LTD and cerebellar learning by Purkinje cell-specific ablation of cGMP-dependent protein kinase I. *J Cell Biol* 163:295–302.
25. Ito M (2001) Cerebellar long-term depression: Characterization, signal transduction, and functional roles. *Physiol Rev* 81:1143–1195.
26. Linden DJ, Connor JA (1992) Long-term depression of glutamate currents in cultured cerebellar Purkinje neurons does not require nitric oxide signaling. *Eur J Neurosci* 4:10–15.
27. Ito M (2002) The molecular organization of cerebellar long-term depression. *Nat Rev Neurosci* 3:896–902.
28. Katoh A, Kitazawa H, Itohara S, Nagao S (2000) Inhibition of nitric oxide synthesis and gene knockout of neuronal nitric oxide synthase impaired adaptation of mouse optokinetic response eye movement. *Learn Mem* 7:220–226.
29. Nagao S, Ito M (1991) Subdural application of hemoglobin to the cerebellum blocks vestibuloocular reflex adaptation. *NeuroReport* 2:193–196.
30. Shutoh F, *et al.* (2006) Memory trace of motor learning shifts transsynaptically from cerebellar cortex to nuclei for consolidation. *Neuroscience* 139:767–777.
31. Kassardjian CD, *et al.* (2005) The site of a motor memory shifts with consolidation. *J Neurosci* 25:7979–7985.
32. Chapman PF, Atkins CM, Allen MT, Haley JE, Steinmetz JE (1992) Inhibition of nitric oxide synthesis impairs two different forms of learning. *NeuroReport* 3:567–570.
33. Kriegsfeld LJ, *et al.* (1991) Nocturnal motor coordination deficits in neuronal nitric oxide synthase knock-out mice. *Neuroscience* 89:311–315.
34. Yanagihara D, Kondo I (1996) Nitric oxide plays a key role in adaptive control of locomotion in cat. *Proc Natl Acad Sci USA* 93:13292–13297.
35. Kim JJ, Thompson RF (1997) Cerebellar circuits and synaptic mechanisms involved in classical eyeblink conditioning. *Trends Neurosci* 20:177–181.
36. Aiba A, *et al.* (1994) Deficient cerebellar long-term depression and impaired motor learning in mGluR1 mutant mice. *Cell* 79:377–388.
37. Kishimoto Y, *et al.* (2001) Impaired delay but normal trace eyeblink conditioning in PLCβ4 mutant mice. *NeuroReport* 12:2919–2922.
38. Kishimoto Y, *et al.* (2001) Classical eyeblink conditioning in glutamate receptor subunit δ2 mutant mice is impaired in the delay paradigm but not in the trace paradigm. *Eur J Neurosci* 13:1249–1253.
39. Kishimoto Y, *et al.* (2002) mGluR1 in cerebellar Purkinje cells is required for normal association of temporally contiguous stimuli in classical conditioning. *Eur J Neurosci* 16:2416–2424.
40. Shibuki K, *et al.* (1996) Deficient cerebellar long-term depression, impaired eyeblink conditioning, and normal motor coordination in GFAP mutant mice. *Neuron* 16:587–599.
41. Eto M, Bock R, Brautigan DL, Linden DJ (2002) Cerebellar long-term synaptic depression requires PKC-mediated activation of CPI-17, a myosin/moesin phosphatase inhibitor. *Neuron* 36:1145–1158.
42. Launey T, *et al.* (2004) Protein phosphatase 2A inhibition induces cerebellar long-term depression and declustering of synaptic AMPA receptor. *Proc Natl Acad Sci USA* 101:6766–6781.
43. Takeuchi T, *et al.* (2008) Enhancement of both long-term depression induction and optokinetic response adaptation in mice lacking delphilin. *PloS ONE* 3:e2297.
44. Ito M (2006) Cerebellar circuitry as a neuronal machine. *Prog Neurobiol* 78:272–303.
45. Stipanovich A, *et al.* (2008) A phosphatase cascade by which rewarding stimuli control nucleosomal response. *Nature* 453:879–884.
46. Osoegawa K, *et al.* (2000) Bacterial artificial chromosome libraries for mouse sequencing and functional analysis. *Genome Res* 10:116–128.
47. Gomi H, *et al.* (1995) Mice devoid of the glial fibrillary acidic protein develop normally and are susceptible to scrapie prions. *Neuron* 14:29–41.
48. Bradford MM (1976) A rapid and sensitive method for the quantitation of microgram quantities of protein utilizing the principle of protein-dye binding. *Anal Biochem* 72:248–254.

Developmental Cell
Article

Committed Neuronal Precursors Confer Astrocytic Potential on Residual Neural Precursor Cells

Masakazu Namihira,[1,5] Jun Kohyama,[1] Katsunori Semi,[1] Tsukasa Sanosaka,[1] Benjamin Deneen,[2] Tetsuya Taga,[3,4] and Kinichi Nakashima[1,*]
[1]Laboratory of Molecular Neuroscience, Graduate School of Biological Sciences, Nara Institute of Science and Technology, 8916-5 Takayama, Ikoma, Nara 630-0101, Japan
[2]Division of Biology 216-76, California Institute of Technology, Pasadena, CA 91125, USA
[3]Division of Cell Fate Modulation, Institute of Molecular Embryology and Genetics, Kumamoto University, 2-2-1 Honjo, Kumamoto 860-0811, Japan
[4]Department of Stem Cell Regulation, Medical Research Institute, Tokyo Medical and Dental University, 1-5-45, Yushima, Bunkyo-ku, Tokyo, 113-8510, Japan
[5]Present address: Department of Human Genetics, David Geffen School of Medicine, University of California at Los Angeles, Los Angeles, CA 90095, USA
*Correspondence: kin@bs.naist.jp
DOI 10.1016/j.devcel.2008.12.014

SUMMARY

During midgestation, mammalian neural precursor cells (NPCs) differentiate only into neurons. Generation of astrocytes is prevented at this stage, because astrocyte-specific gene promoters are methylated. How the subsequent switch from suppression to expression of astrocytic genes occurs is unknown. We show in this study that Notch ligands are expressed on committed neuronal precursors and young neurons in mid-gestational telencephalon, and that neighboring Notch-activated NPCs acquire the potential to become astrocytes. Activation of the Notch signaling pathway in midgestational NPCs induces expression of the transcription factor nuclear factor I, which binds to astrocytic gene promoters, resulting in demethylation of astrocyte-specific genes. These findings provide a mechanistic explanation for why neurons come first: committed neuronal precursors and young neurons potentiate remaining NPCs to differentiate into the next cell lineage, astrocytes.

INTRODUCTION

Fetal telencephalic neuroepithelial cell populations in mammalian embryonic brain contain multipotent neural precursor cells (NPCs) that can self-renew and give rise to the three major central nervous system (CNS) cell types—neurons, astrocytes, and oligodendrocytes. However, NPCs do not express multipotentiality in early gestation, differentiating only into neurons at midgestation; they gradually begin to display multipotentiality, and differentiate into astrocytes and oligodendrocytes during late gestation (Temple, 2001). The mechanisms driving this stepwise process in the developing brain are poorly understood, although cytokine-induced activation of the janus kinase (JAK)-signal transducer and activator of transcription (STAT) pathway, and changes in DNA methylation of astrocyte-specific gene promoters, are thought to be intimately involved in the regulation of astrogliogenesis (Fan et al., 2005; He et al., 2005; Takizawa et al., 2001).

Since neurons are produced before NPCs gain the potential to differentiate into astrocytes, pregenerated neurons are strong candidates to confer astrogliogenic potential on NPCs. In this context, it has been suggested that neuron-secreted cardiotrophin (CT)-1, a member of the interleukin (IL)-6 cytokine family that activates the gp130-JAK-STAT pathway, induces astrocytic differentiation of mouse NPCs at embryonic day (E) 13.5 (Barnabe-Heider et al., 2005). These findings do not, however, exclude the possibility that, prior to E13.5, cortical precursors undergo an intrinsic change, such as demethylation of astrocytic gene promoters (Takizawa et al., 2001), that allows them to respond to cytokines.

Notch receptors and their ligands, molecules best known for influencing cell fate decisions through direct cell-cell contact (Louvi and Artavanis-Tsakonas, 2006; Nye and Kopan, 1995; Weinmaster, 1997), participate in a wide variety of biological events, including fate decision of NPCs. Upon ligand binding, the intracellular domain of Notch (NICD) is released from the plasma membrane and translocates into the nucleus, where it converts the CBF1(RBP-J)/Su(H)/LAG1 (CSL) repressor complex into an activator complex. The NICD/CSL1 activator complex targets genes such as *Hes* and *Hesr* (Hes-related protein), which encode basic helix-loop-helix transcriptional regulators that antagonize proneural genes, and thus neurogenesis (Bertrand et al., 2002; Kato et al., 1997). However, it is largely unknown how the Notch signaling pathway is involved in neurogenic-to-gliogenic switching during CNS development.

Recently, it has been reported that nuclear factor I (NFI) A, a member of a family of CCAAT box element-binding transcription factors (Gronostajski, 2000), is both necessary and sufficient to promote glial fate specification in embryonic spinal cord progenitors in vivo (Deneen et al., 2006). Previous studies had shown that adult mice deficient for NFIA or NFIB exhibited